

Article

Multi-Feedback Interference Cancellation Algorithms for OFDM Systems over Doubly-Selective Channels

Peng Li ^{1,2,*}, Min Chen ³, Li (Alex) Li ^{4,*} and Jiao Feng ^{1,2}

¹ College of Electronic and Information Engineering, Nanjing University of Information Science & Technology, 219 Ningliu Road, Nanjing 210044, China

² Jiangsu Collaborative Innovation Center on Atmospheric Environment and Equipment Technology (CICAEET), Nanjing 210044, China; E-Mail: jiao.feng@nuist.edu.cn

³ College of Information Science and Technology, Hainan University, Haikou 570228, China; E-Mail: excide@126.com

⁴ School of Communication Engineering, Chengdu University of Information Technology, Chengdu 610225, China

* Authors to whom correspondence should be addressed; E-Mails: peng.li@nuist.edu.cn (P.L.); lili1984@163.com (L.L.); Tel.: +86-152-6182-9183 (P.L.); +86-183-8021-0997 (L.L.).

Academic Editor: Evangelos Kranakis

Received: 28 May 2015 / Accepted: 8 July 2015 / Published: 14 July 2015

Abstract: Orthogonal frequency-division multiplexing (OFDM) systems over rapidly time varying channels may suffer from significant inter-carrier interference (ICI), which destroys the orthogonality between subcarriers and degrades the detection performance. Without sufficient ICI suppression, OFDM systems usually experience an error floor. According to the approximate matched filter bound (AMFB), the error floor in a coded OFDM system is not irreducible. In this work, we introduce novel multiple feedback matched filter (MBMF)-based ICI cancellation receivers. Based on the output of a novel MBMF scheme, the approach employs a multiple ICI cancellation strategy with or without signal-to-interference-plus-noise-ratio (SINR) ordering. The developed schemes can significantly improve the performance and remove the error floor with a negligible complexity increase. Given the multiple cancellation approach, we compare the SINR performance of the MBMF outputs with that employing single feedback and show that the SINR performance with multiple cancellation candidates is improved over that with a single one at practical SNR values. Additionally, for time-varying channels, we exploit partial fast Fourier transform (PFFT) by splitting one OFDM symbol into multiple segments; the

channel state is separately estimated by least-squares (LS) methods without inserting more pilots. Simulation results demonstrate the superiority of the proposed methods over serial and block equalizers and the robustness to the Doppler effects compared to conventional single-segment method.

Keywords: interference cancellation; OFDM; doubly-selective channels

1. Introduction

Due to the OFDM system's high spectral efficiency and simple equalization, it has been widely adopted by many digital communication standards, such as Long-term evolution (LTE), LTE-Advanced and Worldwide Interoperability for Microwave Access (WiMAX). However, its performance suffers severely from inter-carrier interference (ICI) caused by the Doppler effect. The ICI can be effectively eliminated by introducing short OFDM symbols. However, the spectral efficiency is reduced due to more cyclic-prefixes (CPs) being required. In order to address this issue, several equalization techniques ranging from linear (zero-forcing (ZF) and minimum mean square error (MMSE)) to non-linear ones (successive interference cancellation (SIC) and (Maximum a priori probability (MAP)) have been proposed. A simple frequency domain ZF equalizer using the banded channel structure has been proposed in [1]; recursive MMSE filters with decision feedback equalization and matched filter bound (MFB) (perfect removal of ICI cancellation) [2,3] have been investigated, and the bound can be considered as the performance benchmark for ICI cancellation algorithms. In [4,5], the authors, using time-domain receiver windowing, further exploited the banded channel matrix in the frequency domain to design the serial and block equalizers with low complexity. Another method, based on the modified banded structure in the time or the frequency domain, estimates the symbols using a sequential least-square QR (LSQR) algorithm with selective parallel interference cancellation (PIC) [6]. Furthermore, the authors in [7,8] proposed two pre-equalizers to mitigate the effects of time variations and to obtain a diagonal channel matrix. One in [7] developed a partial FFT (PFFT) method to reduce the size of receive signal vectors for simple equalization, and the other in [8] has formulated the pre-equalizer based on ICI power minimization. In [9], ICI is modeled using derivatives of the channel amplitude, and an iterative decision feedback equalizer (DFE) was used to derive a single tap equalizer in the frequency domain. A similar idea is implemented in [10] to obtain the diagonal matrix using mean values of transmit symbols based on log-likelihood ratio (LLR) values from the channel decoder. Some other iterative processing techniques employing a novel LLR criterion, hybrid processing or multiple cancellation orders are presented in [11–13]. Additionally, a low-complexity sequential MAP detector using the Markov chain Monte Carlo (MCMC) algorithm for mobile OFDM can be found in [14] with a successively-reduced search dimension using soft ICI cancellation, which is a variant of ICI cancellation with the aid of MAP detection. However, by introducing the Gibbs sampler, the complexity of generating samples for MAP detection is almost the same as that of tens of sequential ICI cancellations with a relatively large channel matrix. Besides the MCMC-MAP equalizer mentioned above, the authors

in [3,15] further investigate the reduced state MAP equalization techniques for uncoded and coded OFDM systems to achieve the benchmarking performance with hardware-realizable complexity. Due to the difficulty of estimating the rapidly varying channel, some joint receiver designs incorporating channel estimation have been proposed for OFDM systems in [16–18]. The authors of [16] propose a successive interference cancellation (SIC) scheme based on a group of subcarriers, namely match filter (MF)-SIC, with iterative single-burst channel estimation (SBCE), but its working scenario is limited to relatively low normalized Doppler frequencies due to the channel estimation error and the residual ICI inside the band. The work presented in [18] is relatively robust to channel time variation, but it requires a higher complexity than others. The recent work in [17] suggests an alternative way of estimating time varying channels in multi-segmental form with soft PIC, which can extend the operation of OFDM systems to higher Doppler frequencies. All of the techniques discussed above consider only the dominant ICI terms inside the band; the rest of the ICI outside the band is treated as white noise. However, the ICI terms outside the band are not properly modeled as white noise, but correlated. Hence, the autocorrelation function of the ICI outside the band has been discussed in [19] to design a pre-whitener to compensate ICI outside the band, the autocorrelation matrix of which can also be applied to the likelihood function for more accurate LLR computations. However, this makes the LLR computations not a desirable feature for soft ICI cancellation.

In this paper, we first discuss the matched filter-based multiple PIC (MF-PIC), and then, we employ multi-feedback ICI cancellation matched filter in a sequential form (MF-SIC). It is worth to noting that the matched filter is used for the proposed methods throughout the paper unless otherwise specified. The original idea is motivated by [20], which proposes multi-feedback (MB) cancellation for MIMO systems to approximate the ML solution by selecting one SIC solution out of multiple candidates. Unlike the work in [14,16,17,20], the proposed multi-feedback matched filter (MBMF) strategy has been employed to approximate the residual ICI induced by soft cancellation and to obtain more reliable LLR values of transmitted bits. We propose two generation mechanisms for the multi-feedback strategy: Gibbs sampling-based generation (GSG) and tree search-based generation (TSG). Note that the generation of feedback candidates by GSG is performed bit by bit independently, unlike the recursive implementation described in [21,22]. Furthermore, it does not require a burn-in period to reach its stationary distribution [14] and the removal of repetitions [23]. For TSG-based on the conventional Bayesian framework, it builds up a tree structure-like breadth-first search algorithm [24] and searches for the most likely candidates given the probability of bits. Hence, the contribution of this paper can be summarized as:

- The effectiveness of MF-PIC and MF-SIC using the banded channel matrix is analytically validated in terms of signal-to-interference-plus-noise-ratio (SINR).
- We propose two generation mechanisms for the multi-feedback strategy: Gibbs sampling-based generation (GSG) and tree search-based generation (TSG).
- The SINR ordering is also discussed to further remove the error floor induced by the ICI.
- With the aid of the autocorrelation of the residual ICI, analytical derivation of the bit error rate (BER) performance with the proposed MBMF scheme is given.
- The derivation of the proposed channel estimation (Multi-segment channel estimation (MSCE)) and the lower MSE performance bound have been presented.

The proposed ICI cancellation algorithms incorporating MSCE show the robustness to the time-varying channels and better performance than other cancellation techniques.

The paper is organized as follows. Section 2 states the system model and receiver structure. Section 3 discusses conventional PIC and SIC for OFDM systems over time-varying channels. Section 4 formulates the problem of multiple interference cancellation and derives its LLR computation. The multi-feedback generation mechanism is presented in Section 5, and the analytical derivation of the BER performance is presented in Section 6. The SINR ordering for MBMF-SIC is in Section 7. Followed by Section 7, the MSCE and the lower bound are investigated in Section 8. In Section 9, the complexity requirement of the interference cancellation and channel estimation algorithms is presented. The simulation results are given in Section 10, and Section 11 draws the conclusions.

2. System Model

We consider a coded OFDM system with N_s subcarriers and iterative processing as illustrated in Figure 1. For a conventional SIC receiver, the number of feedback candidates is reduced to one in the multi-feedback generation block. The information bits are encoded as b_m by the channel encoder and then interleaved as u_m through the random interleaver, where the subscript m denotes the m -th bit in the sequence. Each group of c bits is modulated by the symbol mapper onto one symbol s_k on the k -th subcarrier at the i -th OFDM symbol, and then, the inverse fast Fourier transform (IFFT) is performed to obtain the serial data stream. Hence, the signals can be written as:

$$a_n = \frac{1}{\sqrt{N_s}} \sum_{k=0}^{N_s-1} s_k e^{j \frac{2\pi}{N_s} kn} \tag{1}$$

where the quantity a_n is transmitted over a time-varying multi-path channel. The cyclic-prefix (CP) is inserted after Equation (1). Once the distorted transmitted signals reach the receiver, the CP is removed. Then, the received signals during the i -th OFDM symbol are represented as:

$$r_n = \sum_{l=0}^{L-1} h_{tl}(n, l) a_{n-l} + z_n \quad 0 \leq n < N_s - 1 \tag{2}$$

where the quantity z_n denotes one sample of additive white Gaussian noise (AWGN). The received signals are split into several segments, which go through the PFFT for channel estimation. The summation of the outputs of PFFT blocks is the same as the conventional FFT. Thus, the output is used for equalization as used in conventional OFDM systems. We assume that the k -th subcarrier is the desired one and omit the noise for simplicity. Substituting Equation (1) into Equation (2), Equation (2) after FFT becomes [4]:

$$\begin{aligned}
 y_k &= \frac{1}{N_s} \sum_{n=0}^{N_s-1} \sum_{l=0}^{L-1} \sum_{q=0}^{N_s-1} h_{tl}(n, l) s(q) e^{j2\pi(qn+ql)/N_s} e^{-j2\pi kn/N_s} \\
 &= \underbrace{h_{df}(0, k) s(k)}_{\text{desired signal}} + \underbrace{\sum_{q=0, q \neq k}^{N_s-1} h_{df}(k - q, q) s(q)}_{\text{ICI components}},
 \end{aligned} \tag{3}$$

where $h_{df}(k - q, q) = \frac{1}{N_s} \sum_{n=0}^{N_s-1} \sum_{l=0}^{L-1} h_{tl}(n, l)e^{-j2\pi((k-q)n+ql)/N_s}$, and the quantity $h_{tl}(n, l)$ denotes the channel impulse response for the n -th time index in one OFDM symbol and the l -th channel path. If we let $d = k - q$ and $k = q$, $h_{df}(d, k) = \frac{1}{N_s} \sum_{n=0}^{N_s-1} \sum_{l=0}^{L-1} h_{tl}(n, l)e^{-j2\pi(dn+kl)}$. As described in [4], the quantities d and k in $h_{df}(d, k)$ can be interpreted as the ‘‘Doppler’’ index and the subcarrier index, respectively. We can also rewrite Equation (3) in a matrix form:

$$\mathbf{y} = \underbrace{\mathbf{F}\mathbf{H}_{df}\mathbf{F}^H}_{\mathbf{H}_{df}} \mathbf{s} + \mathbf{v}, \tag{4}$$

where the matrix $\mathbf{H}_{df} \in \mathbb{C}_{N_s \times N_s}$ is illustrated as a circulant matrix in the time domain, and $\mathbf{s} \in \mathbb{C}_{N_s \times 1}$, $\mathbf{y} \in \mathbb{C}_{N_s \times 1}$, $\mathbf{v} \in \mathbb{C}_{N_s \times 1}$, $\mathbf{F} \in \mathbb{C}_{N_s \times N_s}$. The symbol $\mathbb{C}_{n \times n}$ denotes the matrix with the size of n by n .

The matrix \mathbf{H}_{df} denotes the equivalent frequency channel matrix with the size of $N_s \times N_s$. The output of MBMF block is the output of the equalizer, which yields the estimated symbols \hat{s}_k . The bit LLRs corresponding to these symbols can be obtained and deinterleaved for the channel decoder using the MAP algorithm [25]. The output of the channel decoder, after the interleaver, is also used for the interference cancellation. The interference is regenerated by the multi-feedback generation block. For the conventional SIC receiver, the number of feedback candidates is reduced to one in the output of the multi-feedback generation block. In the following, the processing is based on the frequency domain, unless otherwise specified.

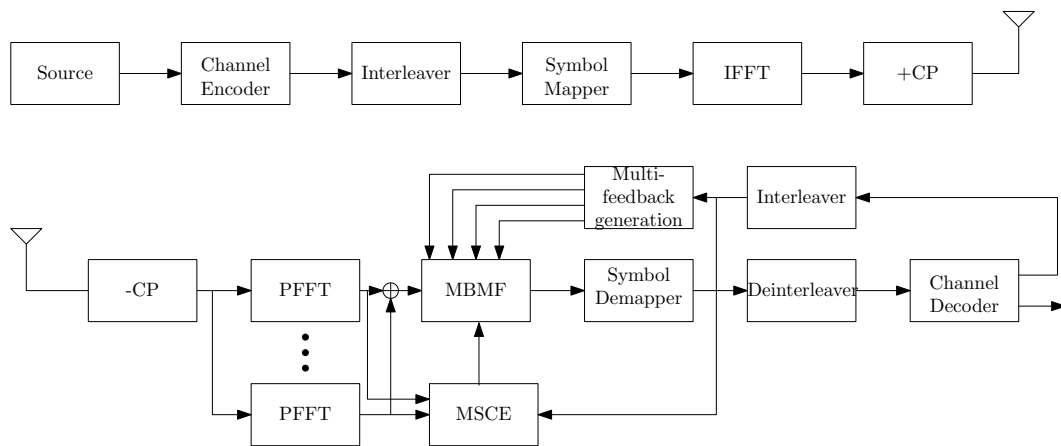


Figure 1. System model of multiple feedback matched filter (MBMF)-successive interference cancellation (SIC) incorporating multi-segment channel estimation (MSCE).

We employ a banded channel matrix $\mathbf{H}_D \in \mathbb{C}_{N_s \times N_s}$ for OFDM systems over doubly-selective channels, as shown in Figure 2 and [4], so the truncated system model for the k -th subcarrier can be approximated as below:

$$\begin{aligned} \mathbf{y}_k &= \mathbf{H}_k \mathbf{s}_k + \mathbf{v}_k \\ &= \mathbf{h}_k s_k + \sum_{\bar{k}=k-Q, \bar{k} \neq k}^{k+Q} \mathbf{h}_{\bar{k}} s_{\bar{k}} + \sum_{\bar{k} \notin [k-Q, k+Q]} \mathbf{h}_{\bar{k}} s_{\bar{k}} + \mathbf{v}_k \end{aligned} \tag{5}$$

where the truncated received signal is given by $\mathbf{y}_k = [y_{k-D}, \dots, y_k, \dots, y_{k+D}]^T$, \mathbf{h}_k denotes the k -th column vector of the truncated channel matrix, the truncated transmit symbol vector for the k -th subcarrier is $\mathbf{s}_k = [s_{k-2D}, \dots, s_k, \dots, s_{k+2D}]^T$, the truncated noise vector is expressed by $\mathbf{v}_k = [v_{k-D}, \dots, v_k, \dots, v_{k+D}]$ and the truncated channel matrix \mathbf{H}_k has a size $Q = 2D$, as illustrated in Figure 2.

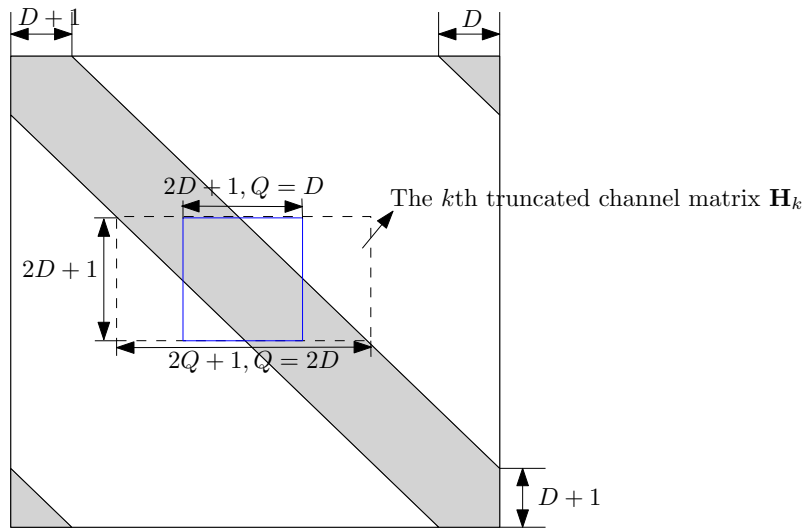


Figure 2. The matrix representations of the banded channel matrix \mathbf{H}_D , the k -th truncated channel matrix \mathbf{H}_k and the reduced channel matrix in the blue square.

3. Matched Filter Parallel Interference Cancellation

In this section, we present a MF-PIC approach to mitigate the ICI in OFDM systems. The banded structure is employed to reduce the complexity of MF-PIC in the matched filtering stage and the cancellation stage. This is because the elements of \mathbf{H}_D outside the shaded area are omitted for complexity reduction. The LLR calculation of MF-PIC is also discussed as follows. The ICI terms are mostly contributed by $2Q$ adjacent subcarriers, as illustrated in Figure 2 and reported in [4]. Hence, the residual ICI outside the band is considered as noise. The matched filtered signals are expressed as follows:

$$\begin{aligned} \hat{\mathbf{y}} &= \mathbf{H}_D^H \mathbf{y} \\ &= \mathbf{H}_D^H \mathbf{H}_{df} \mathbf{s} + \mathbf{H}_D \mathbf{v} \\ &= \mathbf{R}_{Df} \mathbf{s} + \tilde{\mathbf{v}}, \end{aligned} \tag{6}$$

where the vector $\hat{\mathbf{y}} = [\hat{y}_0, \dots, \hat{y}_k, \dots, \hat{y}_{N_s-1}]^T$ represents the MF outputs. We consider the quadrature phase shift keying (QPSK) here to simplify the exposition, even though we remark that it is straightforward to generalize the LLR processing to other constellations. Hence, the LLR values of $s_k(i), i = 1, 2$ for the channel decoder and the soft symbol estimates for iterative interference cancellation can be computed as [16]:

$$\mathbf{L}(s_k(1)) = \ln \frac{\Pr(s_k(1) = +1 | \hat{y}_k)}{\Pr(s_k(1) = -1 | \hat{y}_k)} = \frac{4\Re(\hat{y}_k)}{\sigma_v^2} \tag{7}$$

Accordingly, $L(s_k(1)) = \frac{4\mathfrak{S}(\hat{y}_k)}{\sigma_v^2}$, where the quantity $s_k(i)$ denotes the i -th bit of the symbol s_k at the k -th subcarrier, and $i = 1, 2$, because QPSK symbols carry two information bits. Subsequently, $L(s_k(i))$ from Equation (7) is deinterleaved and then fed to the channel decoder as the *a priori* LLRs. The extrinsic LLRs of $L(s_k(i))$ can be obtained from the channel decoder, and then, the soft symbol estimates \hat{s}_k are fed back for soft interference cancellation after the interleaver, as given in Equation (8). The received data vector after cancellation is given by:

$$\bar{\mathbf{y}} = \hat{\mathbf{y}} - \tilde{\mathbf{R}}_{Df}\hat{\mathbf{s}}, \tag{8}$$

where $\bar{\mathbf{y}} = [\bar{y}_0, \dots, \bar{y}_k, \dots, \bar{y}_{N_s-1}]^T$, $\hat{\mathbf{s}} = [\hat{s}_0, \dots, \hat{s}_k, \dots, \hat{s}_{N_s-1}]^T$, $\tilde{\mathbf{R}}_{Df}$ is the matrix with zero diagonal elements, and the new LLR value $L(s_k(i))$ can be re-computed in Equation (7) to replace \hat{y}_k by \bar{y}_k . According to Bayes's theorem [26] and Equation (7), the soft symbol estimate of the k -th subcarrier for interference cancellation is given by:

$$\hat{s}_k = \tanh(L(s_k(1))/2) + \tanh(L(s_k(2))/2)i, \tag{9}$$

where $\sqrt{-1} = i$. Therefore, the MF-PIC can cancel the ICI in one shot once the *a priori* LLR from the channel decoder is known and then fed the new LLR after the ICI cancellation to the channel decoder.

4. Proposed Multi-Feedback Interference Cancellation

Motivated by the algorithm presented in Section 3, we discuss the basic idea of multi-feedback interference cancellation in this section and compare it with the conventional soft interference cancellation and MAP detector via LLR representation. This implies that the proposed multi-feedback interference cancellation algorithm can be considered as a hybrid detection method performing multiple ICI suppression operations simultaneously for the desired subcarrier.

4.1. Problem Formulation and Solution

The received signal in Equation (5) after subtracting the soft symbol estimates is given by:

$$\tilde{\mathbf{y}}_k = \mathbf{h}_k s_k + \underbrace{\sum_{\bar{k}=k-Q, \bar{k} \neq k}^{k+Q} \mathbf{h}_{\bar{k}}(s_{\bar{k}} - \hat{s}_q)}_{\text{soft residual interference inside band}} + \underbrace{\sum_{\bar{k} \notin [k-Q, k+Q]} \mathbf{h}_{\bar{k}} s_{\bar{k}} + \mathbf{v}_k}_{\tilde{\mathbf{v}}}, \tag{10}$$

where $\hat{\mathbf{s}}_{\bar{k}} = [s_{k-Q}, \dots, \hat{s}_{k-1}, \hat{s}_{k+1}, \dots, s_{k+Q}]^T$, $\hat{s}_q \in \hat{\mathbf{s}}_{\bar{k}}$ denotes the soft symbol vector omitting the desired symbol at the k -th subcarrier \hat{s}_k , which are inside the band obtained by previously-detected subcarriers or the LLR from the channel decoder. The vector $\tilde{\mathbf{v}}$ denotes the interference outside the band plus noise. The residual interference inside the band can be approximated by the summation of received signals $\tilde{\mathbf{y}}_k^{(b)}$, $b = 1, 2, \dots, B$, after subtracting multiple interference symbols $s_{\bar{k}}^{(b)}$ as follows:

$$\sum_{\bar{k}=k-Q, \bar{k} \neq k}^{k+Q} \mathbf{h}_{\bar{k}}(s_{\bar{k}} - \hat{s}_{\bar{k}}) \approx \sum_{b=1}^B (\tilde{\mathbf{y}}_k^{(b)} - \mathbf{h}_k s_k - \tilde{\mathbf{n}}) \Pr(\tilde{\mathbf{y}}_{\bar{k}}^{(b)}), \tag{11}$$

where:

$$\tilde{\mathbf{y}}_k^{(b)} = \mathbf{h}_k s_k + \underbrace{\sum_{\substack{\bar{k}=k-Q, \bar{k} \neq k \\ \bar{k}=k+Q, \bar{k} \neq k}} \mathbf{h}_{\bar{k}} (s_{\bar{k}} - s_{\bar{k}}^{(b)})}_{\text{hard residual interference inside band}} + \tilde{\mathbf{v}}, \quad (12)$$

and $\mathbf{s}_{\bar{k}}^{(b)} = [s_{k-Q}^{(b)}, \dots, s_{k-1}^{(b)}, s_{k+1}^{(b)}, \dots, s_{k+Q}^{(b)}]^T$, $s_{\bar{k}}^{(b)} \in \mathbf{s}_{\bar{k}}^{(b)}$. The quantity B denotes the number of feedback candidates. Substituting Equation (11) into Equation (10), we arrive at:

$$\mathbf{y}_k^* \approx \tilde{\mathbf{y}}_k - \sum_{b=1}^B (\tilde{\mathbf{y}}_k^{(b)} - \mathbf{h}_k s_k - \tilde{\mathbf{v}}) \Pr(\tilde{\mathbf{y}}_k^{(b)}) \approx \mathbf{h}_k s_k + \tilde{\mathbf{v}}, \quad (13)$$

where \mathbf{y}_k^* denotes the received signal if the residual interference inside the band is perfectly removed by Equation (11), and the probability $\Pr(\mathbf{y}_k^{(b)})$ denotes the *a priori* probability of received signals after interference cancellation, which are mainly determined by $\Pr(\mathbf{s}_{\bar{k}}^{(b)})$. Hence, the terms $\Pr(\mathbf{y}_k^{(b)})$ and $\Pr(\mathbf{s}_{\bar{k}}^{(b)})$ are interchangeable ($\Pr(\tilde{\mathbf{y}}_k^{(b)}) \approx \Pr(\mathbf{s}_{\bar{k}}^{(b)})$). If we assume no residual interference inside the band in Equation (13) after a rearrangement, it becomes:

$$\tilde{\mathbf{y}}_k - \sum_{b=1}^B \tilde{\mathbf{y}}_k^{(b)} \Pr(\tilde{\mathbf{y}}_k^{(b)}) = \mathbf{h}_k s_k + \tilde{\mathbf{v}} - \mathbf{h}_k s_k \sum_{b=1}^B \Pr(\tilde{\mathbf{y}}_k^{(b)}) - \tilde{\mathbf{v}} \sum_{b=1}^B \Pr(\tilde{\mathbf{y}}_k^{(b)}), \quad (14)$$

where $\sum_{b=1}^B \Pr(\tilde{\mathbf{y}}_k^{(b)}) = \sum_{b=1}^B \Pr(\mathbf{s}_{\bar{k}}^{(b)}) \approx 1$, if all possible combinations of symbol vectors $\mathbf{s}_{\bar{k}}^{(b)}$ are considered in the summation. Therefore, $\tilde{\mathbf{y}}_k - \sum_{b=1}^B \tilde{\mathbf{y}}_k^{(b)} \Pr(\tilde{\mathbf{y}}_k^{(b)}) \approx 0$. Note that the conditional probability of $\tilde{\mathbf{y}}_k^{(b)}$ given $\mathbf{s}_{\bar{k}}^{(b)}$ and $\tilde{\mathbf{y}}_k$ given $\hat{\mathbf{s}}_{\bar{k}}$ in Equation (14) will be mutually exclusive and conditionally independent, if the residual interference term dominates. Hence, the likelihood functions of $\tilde{\mathbf{y}}_k^{(b)}$ and $\tilde{\mathbf{y}}_k$ given s_k can be separately evaluated by:

$$\Pr(\tilde{\mathbf{y}}_k^{(b)} | s_k) \propto e^{-\frac{(\tilde{\mathbf{y}}_k^{(b)} - \mathbf{h}_k s_k)^H}{\sigma_v^2} (\tilde{\mathbf{y}}_k^{(b)} - \mathbf{h}_k s_k)} \quad (15)$$

For simplicity, we assume QPSK is used as in the previous subsection, so $s_k(i) = \pm 1, i = 1, 2$. Using Equation (15), the LLR can be computed as:

$$L(s_k^{(b)}(1)) = \ln \frac{\Pr(s_k(1) = +1 | \tilde{\mathbf{y}}_k^{(b)})}{\Pr(s_k(1) = -1 | \tilde{\mathbf{y}}_k^{(b)})} = \frac{4\Re(\mathbf{h}_k^H \tilde{\mathbf{y}}_k^{(b)})}{\sigma_v^2}, \quad (16)$$

and the conditional probability of $s_k^{(b)}(1)$ given $\tilde{\mathbf{y}}_k^{(b)}$ can be calculated by:

$$\Pr(s_k^{(b)}(1) = +1 | \tilde{\mathbf{y}}_k^{(b)}) = \frac{1}{1 + e^{-L(s_k^{(b)}(1))}} \quad (17)$$

Accordingly, $L(s_k^{(b)}(2)) = \frac{4\Im(\mathbf{h}_k^H \tilde{\mathbf{y}}_k^{(b)})}{\sigma_v^2}$. From Equation (17), multiple conditional probabilities $\Pr(s_k^{(b)}(1) = +1 | \tilde{\mathbf{y}}_k^{(b)})$ and $\Pr(s_k(1) = +1 | \tilde{\mathbf{y}}_k)$ can be obtained. Hence, the average conditional probability $\Pr(s_k | \mathbf{y}_k^*)$ can be obtained by:

$$\Pr(s_k(1) = +1 | \mathbf{y}_k^*) = \sum_{b=1}^B \Pr(s_k^{(b)}(1) = +1 | \tilde{\mathbf{y}}_k^{(b)}) \Pr(\tilde{\mathbf{y}}_k^{(b)}) + \Pr(s_k(1) = +1 | \tilde{\mathbf{y}}_k) \Pr(\tilde{\mathbf{y}}_k), \quad (18)$$

As mentioned above, $\Pr(\tilde{\mathbf{y}}_k^{(b)}) = \Pr(\mathbf{s}_k^{(b)})$, which can be obtained by the LLR from the channel decoder. Equation (18) can be rewritten as:

$$\Pr(s_k(1) = +1|\mathbf{y}_k^*) = \sum_{b=1}^B \Pr(s_k^{(b)}(1) = +1|\tilde{\mathbf{y}}_k^{(b)})\Pr(\mathbf{s}_k^{(b)}) + \Pr(s_k(1) = +1|\tilde{\mathbf{y}}_k)\Pr(\hat{\mathbf{s}}_k), \tag{19}$$

The second term in Equation (19) can also be evaluated according to Equation (15). The LLR of $s_k(1)$ for the channel decoder, with the use of Equation (19), can be easily evaluated by:

$$L(s_k(1)) = \ln \frac{\Pr(s_k(1) = +1|\mathbf{y}_k^*)}{\Pr(s_k(1) = -1|\mathbf{y}_k^*)}. \tag{20}$$

Hence, we have obtained the new LLR output by the multi-feedback cancellation algorithm in this section and can further use it in the channel decoder.

4.2. Comparison of Soft Interference Cancellation and MAP Detection

To show the differences between the proposed MBMF-SIC, the MAP and the conventional soft ICI cancellation algorithm, the LLRs of different methods are shown below. For the MAP detection algorithm, the LLR of the i -th particular bit $s_k(i)$ can be found as:

$$L(s_k(i)) = \ln \frac{\sum_{\mathbf{s}_k \in \mathbb{S}_{i+}} \Pr(\mathbf{s}_k|\mathbf{y}_k)}{\sum_{\mathbf{s}_k \in \mathbb{S}_{i-}} \Pr(\mathbf{s}_k|\mathbf{y}_k)}, \tag{21}$$

where $\mathbb{S}_{i\pm}$ denotes the set of different symbol vector combinations \mathbf{s}_k with $s_k(i) = \pm 1$. For soft interference cancellation based on Equation (10), the LLR can be evaluated by:

$$L(s_k(i)) = \ln \frac{\sum_{s_k \in \mathbb{C}_{i+}} \Pr(s_k|\tilde{\mathbf{y}}_k)}{\sum_{s_k \in \mathbb{C}_{i-}} \Pr(s_k|\tilde{\mathbf{y}}_k)}, \tag{22}$$

where $\mathbb{C}_{i\pm}$ denotes the set of different symbol combinations s_k with $s_k(i) = \pm 1$. Given Equations (21) and (22), Equation (18) can be rewritten in the form of an LLR as:

$$L(s_k(i)) \approx \ln \frac{\sum_{\mathbf{s}_{\bar{k}} \in \mathbb{S}_{\bar{k}}} \sum_{s_k \in \mathbb{C}_{i+}} \Pr(s_k|\tilde{\mathbf{y}}_k)\Pr(\tilde{\mathbf{y}}_k|\mathbf{s}_{\bar{k}})\Pr(\mathbf{s}_{\bar{k}})}{\sum_{\mathbf{s}_{\bar{k}} \in \mathbb{S}_{\bar{k}}} \sum_{s_k \in \mathbb{C}_{i-}} \Pr(s_k|\tilde{\mathbf{y}}_k)\Pr(\tilde{\mathbf{y}}_k|\mathbf{s}_{\bar{k}})\Pr(\mathbf{s}_{\bar{k}})}, \tag{23}$$

where $\mathbb{S}_{\bar{k}}$ denotes the set of symbol vector combinations \mathbf{s}_k omitting the symbol s_k , the vector $\tilde{\mathbf{y}}_k$ denotes the received signals suppressing the interference from $\mathbf{s}_{\bar{k}}$ and the vector $\mathbf{y}_{\bar{k}}$ denotes the received signals canceling the desired symbol s_k . Note that the quantity B actually constrains the set size of $\mathbb{S}_{\bar{k}}$. However, the probability $\Pr(\tilde{\mathbf{y}}_k|\mathbf{s}_{\bar{k}})$ may not be tractable in the implementation, so $\Pr(\mathbf{s}_{\bar{k}}) \approx \Pr(\tilde{\mathbf{y}}_k|\mathbf{s}_{\bar{k}})\Pr(\mathbf{s}_{\bar{k}})$ is assumed. Hence, Equation (23) can be considered as another way of implementing the conventional MAP detection in two steps. The first step performs MAP detection for the interference symbols $\mathbf{s}_{\bar{k}}$, and the last step performs interference cancellation for one particular bit $s_k(i)$.

5. Multi-Feedback Generation Mechanism

As mentioned above, the vectors $\hat{s}_{\bar{k}}$ in Equation (10) and $s_k^{(b)}$ in Equation (12) denote the soft symbol vector and the b -th feedback symbol vector, respectively. For soft symbol estimates, it can be obtained by:

$$\hat{s}_{\bar{k}} = \sum_{j=1}^{|\mathbb{C}|} \Pr(s_{\bar{k}} = C_j | \mathbf{y}_k^*) C_j, \tag{24}$$

where C_j denotes the j -th symbol in the symbol alphabet \mathbb{C} . For the generation of $s_k^{(b)}$, there are two different generation methods described below: (1) Gibbs sampler-based generation; (2) tree search-based generation. The algorithm procedure for QPSK is also illustrated in Algorithm 1. It can also be extended to other modulation schemes accordingly. However, it is unlikely that OFDM systems will operate with a high-order modulation scheme in situations of very high mobility.

Algorithm 1 . Proposed MBMF-SIC for QPSK.

Input: $\tilde{\mathbf{y}}_k = \mathbf{y}_k, \mathbf{H}_k, \sigma_n^2, k = 0, 1, \dots, N_s - 1$

Output: $L(s_k(1)), L(s_k(2)), k = 0, 1, \dots, N_s - 1$

- 1: **If** this is the initial iteration, go to step 2. **Else** go to step 9
 - 2: **For** $k = 0, 1, \dots, N_s - 1$
 - 3: **For** $\bar{k} = k - Q, \dots, k - 1, k + 1, \dots, k + Q$ inside the band
 $L(s_{\bar{k}}(1)) = \frac{\Re(\mathbf{h}_{\bar{k}}^H \tilde{\mathbf{y}}_{\bar{k}})}{\sigma_v^2}, L(s_{\bar{k}}(2)) = \frac{\Im(\mathbf{h}_{\bar{k}}^H \tilde{\mathbf{y}}_{\bar{k}})}{\sigma_v^2},$
End
 - 4: Generate feedback symbols $s_{\bar{k}}^b, b = 1, 2, \dots, B$ by GSG or TSG according to log-likelihood ratio (LLR) obtained in step 3 and soft feedback symbols $\hat{s}_{\bar{k}}$ by Equation (24).
 - 5: Perform interference cancellation as Equations (10) and (12) using $s_{\bar{k}}^b, b = 1, 2, \dots, B$ and $\hat{s}_{\bar{k}}$ to obtain $\tilde{\mathbf{y}}_k^{(b)}$ and $\tilde{\mathbf{y}}_k$.
 - 6: Calculate $L(s_k^{(b)}(i))$ and $L(\hat{s}_k(i))$ according to $\tilde{\mathbf{y}}_k^{(b)}$ and $\tilde{\mathbf{y}}_k$ respectively, $i = 1, 2$.
 - 7: Calculate $\Pr(s_k(1) = +1 | \mathbf{y}_k^*)$ and $\Pr(s_k(2) = +1 | \mathbf{y}_k^*)$ as Equation (18) and the corresponding LLR for the cancellation in Equation (10) and the channel decoder.
 - 8: **End**
 - 9: **For** $k = 0, 1, \dots, N_s - 1$
 - 10: **For** $\bar{k} = k - Q, \dots, k - 1, k + 1, \dots, k + Q$ inside the band
Obtain $L(s_{\bar{k}}(i)), i = 1, 2$ from the channel decoder.
End
 - 11: Generate feedback symbols $s_{\bar{k}}^b, b = 1, 2, \dots, B$ by GSG or TSG according to LLR obtained in step 10, and soft feedback symbols $\hat{s}_{\bar{k}}$ by Equation (24).
 - 12: Perform interference cancellation as Equations (10) and (12) using $s_{\bar{k}}^b, b = 1, 2, \dots, B$ and $\hat{s}_{\bar{k}}$ to obtain $\tilde{\mathbf{y}}_k^{(b)}$ and $\tilde{\mathbf{y}}_k$.
 - 13: Calculate $L(s_k^{(b)}(i))$ and $L(\hat{s}_k(i))$ according to $\tilde{\mathbf{y}}_k^{(b)}$ and $\tilde{\mathbf{y}}_k$, respectively, $i = 1, 2$.
 - 14: Calculate $\Pr(s_k(1) = +1 | \mathbf{y}_k^*)$ and $\Pr(s_k(2) = +1 | \mathbf{y}_k^*)$ as Equation (18) and the corresponding LLR for the cancellation in Equation (10) and the channel decoder.
 - 15: **End**
-

5.1. Gibbs Sampling-Based Generation

The bit $s_{\bar{k}}^{(b)}(i)$ can be re-generated by the Gibbs sampler [22]:

$$s_{\bar{k}}^{(b)}(i) = \begin{cases} +1 & \text{if } U(s_{\bar{k}}^{(b)}(i)) \leq P(s_{\bar{k}}^{(b)}(i)) \\ -1 & \text{otherwise} \end{cases}, \quad (25)$$

where $P(s_{\bar{k}}^{(b)}(i)) = \Pr(s_{\bar{k}}(i) = +1 | \mathbf{y}_k^*)$ from the channel decoder, and the notation $U()$ denotes a random number generated based on a uniform distribution between $[0, 1]$. Hence, these bits can be re-mapped onto the symbols C_j . The probability $\Pr(s_{\bar{k}}^{(b)})$ is required for the computation of the average conditional probability in Equation (19). However, the symbol vectors $\mathbf{s}_k^{(b)}$ are randomly generated by Equation (25). Here, we assume an extreme case that the probability $P(s_{\bar{k}}^{(b)}(i)) = 1, \forall b, i$ and the symbol vectors $\mathbf{s}_{\bar{k}}^{(b)}, \forall b$ will be identical. In other words, the Gibbs sampler with reliable feedback from the channel decoder is prone to generate similar symbol vectors, which have almost equal probability ($\Pr(s_{\bar{k}}^{(1)}) \approx \dots \approx \Pr(s_{\bar{k}}^{(b)}) \approx \dots \Pr(s_{\bar{k}}^{(B)}) \approx \Pr(\hat{\mathbf{s}}_{\bar{k}})$). The number of feedback candidates B can approach ∞ for GSG, so $\tilde{\mathbf{y}}_k - \sum_{b=1}^B \tilde{\mathbf{y}}_k^{(b)} \Pr(\tilde{\mathbf{y}}_k^{(b)}) \approx 0$. However, it is undesirable for the implementation to choose a very large B , so a pre-defined B would allow the scheme to achieve an attractive tradeoff between complexity and performance.

5.2. Tree Search-Based Generation

Compared to the Gibbs sampling-based method, feedback can also be generated given the probability of the symbol. For the case of QPSK, the conditional probability can be computed as:

$$\begin{aligned} \Pr(s_{\bar{k}} = C_1 | \mathbf{y}_k^*) &= p_1 p_2 \\ \Pr(s_{\bar{k}} = C_2 | \mathbf{y}_k^*) &= p_1 (1 - p_2) \\ \Pr(s_{\bar{k}} = C_3 | \mathbf{y}_k^*) &= (1 - p_1) p_2 \\ \Pr(s_{\bar{k}} = C_4 | \mathbf{y}_k^*) &= (1 - p_1) (1 - p_2) \end{aligned} \quad (26)$$

where $p_i, i = 1, 2$ denotes the probability $\Pr(s_{\bar{k}}(i) = +1)$ calculated by $L(s_{\bar{k}}(i))$ from the channel decoder. Hence, the most likely symbol combinations can be obtained by calculating and sorting $\Pr(s_{\bar{k}}^{(b)})$, the process of which is similar to the tree search problem in [24]. To further simplify the search process, the computation is performed in the logarithm domain. The search process is implemented as follows:

1. Initialization: $P(C_1^{\bar{k}}) = -\log(p_1 p_2), P(C_2^{\bar{k}}) = -\log(p_1 (1 - p_2)), P(C_3^{\bar{k}}) = -\log((1 - p_1) p_2), P(C_4^{\bar{k}}) = -\log((1 - p_1) (1 - p_2)), \bar{k} = 1, 2, \dots, 2Q, j = 1, 2, \dots, |C|$ and $\Pr(s_{\bar{k}}^{(b)}) = \sum_{\bar{k}=k-Q, \bar{k} \neq k}^{k+Q} P(C_j^{\bar{k}})$, where the quantity $C_j^{\bar{k}}$ denotes the probability of the j -th symbol in the logarithm domain at the \bar{k} -th subcarrier.
2. Solve $\text{argmin}_{\mathbf{s}_{\bar{k}}^{(b)} \in \mathbb{S}_{\bar{k}}} \Pr(s_{\bar{k}}^{(b)}), b = 1, 2, \dots, B$ using the tree search algorithm in [24],
3. Output $\mathbf{s}_{\bar{k}}^{(b)}, b = 1, 2, \dots, B$ and the corresponding weight calculated in Step 2.

The symbol vectors $\mathbf{s}_{\bar{k}}^{(b)}, b = 1, 2, \dots, B$ and the corresponding probability $\Pr(s_{\bar{k}}^{(b)}), b = 1, 2, \dots, B$ can be obtained by the above search. For TSG, the probability $\Pr(\hat{\mathbf{s}}_{\bar{k}})$ is unknown, so Equation (19)

cannot be derived. However, the probability $\Pr(\hat{s}_{\bar{k}})$ can be assumed to be $\frac{1}{B+1}$ as the assumption made in GSG, which is $(\Pr(s_{\bar{k}}^{(1)}) \approx \dots \approx \Pr(s_{\bar{k}}^{(b)}) \approx \dots \Pr(s_{\bar{k}}^{(B)}) \approx \Pr(\hat{s}_{\bar{k}}))$. Hence, $\Pr(s_{\bar{k}}^{(b)}) = \frac{1}{B+1}\Pr(s_{\bar{k}}^{(b)})$ for TSG in Equation (19). Thus, in this section, we have obtained two different multi-feedback generation schemes, which can provide the weighted feedback candidates generated by the *a priori* probability from the channel decoder.

5.3. Further Discussion on Generation Mechanisms

From the above, the contribution of the second term in Equation (18) will be reduced with the increasing number of feedback candidates for both generation mechanisms, and they will converge to the MAP algorithm. However, it requires a larger channel matrix and more candidates as in [14]. The main difference between the Gibbs sampling-based generation and the tree search-based generation is the terms $\Pr(s_{\bar{k}}^{(b)})$ and $\Pr(\hat{s}_{\bar{k}})$. For TSG, the probability $\Pr(\tilde{y}_k^{(b)})$ is calculated with the LLR fed back from the channel decoder. On the other hand, each feedback in GSG is assumed to be equally probable. However, they perform almost identically in BER performance with the same number of feedback candidates. This is because TSG and GSG make use of the LLR from the channel decoder in different forms. The complexity of these two methods is not very intensive. The GSG employs one or multiple random number generators, which can be implemented efficiently without any multiply operations, as stated in [27]. For TSG, multipliers are also not required due to the use of logarithm domain computation. For example, the number of real additions required for TSG is around $2QB|C|$ at most.

5.4. Reduced Channel Matrix for Multi-Feedback Interference Cancellation

Conventionally, the more interference is mitigated, the better the SINR performance achieved. However, the output SINR of a matched filter with a reduced size $Q = D$ channel matrix may not suffer significant performance loss compared to that with a normal-sized $Q = 2D$ channel matrix. According to the statements in [19], the truncated channel matrix can also be reduced to the matrix in blue, as shown in Figure 2. The representation of the reduced channel matrix is illustrated in the blue square. It can be found that the elements in the upper-left corner and lower-right corner have been omitted compared to the matrix with $Q = 2D$

To show the pre-processing SINR difference between the reduced size channel matrix $Q = D$ and the normal-sized channel matrix $Q = 2D$, the pre-processing SINR obtained by observing $\tilde{y}_k^{(b)}$ in Equation (12) is:

$$\begin{aligned} \text{SINR}_Q^{(b)} &\approx \frac{E_s \mathbb{E}\{\mathbf{h}_k^H \mathbf{h}_k\}}{\sum_{q=k-Q, q \neq k}^{k+Q} \mathbb{E}\{\mathbf{h}_k^H \mathbf{h}_k\} |s_{\bar{k}} - s_{\bar{k}}^{(b)}|^2 \bar{P}(s_{\bar{k}}^{(b)}) + \mathbb{E}\{\tilde{\mathbf{n}}_k^H \tilde{\mathbf{n}}_k\}} \\ &\approx \frac{\tilde{E}_s}{\sum_{\bar{k}=k-Q, \bar{k} \neq k}^{k+Q} \mathbb{E}\{\mathbf{h}_k^H \mathbf{h}_k\} |s_{\bar{k}} - s_{\bar{k}}^{(b)}|^2 \bar{P}(s_{\bar{k}}^{(b)}) + \mathbb{E}\{\tilde{\mathbf{n}}_k^H \tilde{\mathbf{n}}_k\}}, \end{aligned} \tag{27}$$

where $\bar{P}(s_q^{(b)}) = \Pr(s_q \neq s_q^{(b)})$, and the quantity E_s denotes the average transmit signal power. Note that the exact symbol error probability $\bar{P}(s_q^{(b)})$ in a coded system cannot be easily obtained. The residual interference term inside the band is omitted for simplicity. Because the first term in the denominator of

Equation (27) will be significantly suppressed at high SNR by the MBMF-SIC, the entire ICI power σ_{c0}^2 and ICI power σ_{cQ}^2 outside Q central terms can be evaluated by an upper bound [19,28] as:

$$\begin{aligned} \sigma_{c0}^2 &\approx \frac{E_s}{12} (2\pi T_{sa} N_s)^2 \left(\sum_{l=0}^{L-1} \sigma_l^2 \sigma_{Dl}^2 \right) - \frac{E_s}{240} (2\pi T_{sa} N_s)^4 \left(\sum_{l=0}^{L-1} \sigma_l^2 \sigma_{Dl}^4 \right) \\ \sigma_{cQ}^2 &\approx \sigma_{c0}^2 \left(1 - \frac{6}{\pi^2} \sum_{q=1}^{2D} \frac{1}{q^2} \right) \end{aligned} \tag{28}$$

where σ_l^2 denotes the variance of the l -th channel tap. $\sigma_{Dl}^2 = \int_{-f_d}^{f_d} P_l(f) f^2 df$, and $P_l(f)$ is the Doppler power spectral density (PSD) of the l -th path. $\sigma_{Dl}^2 = f_d^2/2$, and $\tilde{E}_s = E_s - \sigma_{c2D}^2$ denotes the transmit signal power inside the band with a normal channel matrix $Q = 2D$. The quantity $T_{sa} = \frac{T_{OFDM}}{N_s}$. For $Q = 2D$, Equation (27) can be rewritten as:

$$\text{SINR}_Q^{(b)} \approx \frac{Q \tilde{E}_s}{\mathbb{E}\{\tilde{\mathbf{n}}_k^H \tilde{\mathbf{n}}_k\}} \tag{29}$$

Without the residual interference inside the band, the SINR for the b -th feedback is mainly determined by the noise plus the ICI outside the band. Furthermore, the power of the signal \tilde{E}_s for $Q = D$ will be identical to that for $Q = 2D$, because the power of the desired signal is derived from the same channel coefficients \mathbf{h}_k for $Q = D$ or for $Q = 2D$. Similar to [19], $\text{SINR}_{2D}^{(b)} > \text{SINR}_D^{(b)}$ if no pre-whitener is employed. However, the post-processing SINR of the matched filter \mathbf{h}_k^H will partially contradict the above discussion, which can be evaluated by:

$$\text{PSINR}_Q^{(b)} \approx \frac{\tilde{E}_s^2 / E_s}{\text{tr}(\mathbb{E}\{\mathbf{h}_k \mathbf{h}_k^H\} \mathbb{E}\{\mathbf{c}_k \mathbf{c}_k^H\}) + \sigma_v^2} \tag{30}$$

where the vector $\mathbf{c}_k = [c_{k-D,k} \ c_{k-D+1,k} \ \dots \ c_{k+D,k}]^T$ denotes the residual ICI outside the band for the k -th subcarrier and $c_{k-i,k} = \frac{1}{\sqrt{E_s}} \sum_{\bar{k} \notin [k-Q-i, k+Q-i]} H_{\bar{k}, k-i} s_{\bar{k}}$, which implies that the ICI outside the band interfere with the desired signals at the neighbor subcarriers. The autocorrelation function of the channel coefficients \mathbf{h}_k can be derived by [19]:

$$\begin{aligned} \mathbb{E}\{h_{df}(d, k) h_{df}^*(d+r, k)\} &\approx 4\pi^2 T_{sa}^2 \left(\sum_{l=0}^{N_h-1} \sigma_l^2 \sigma_{Dl}^2 \right) \\ &\cdot \frac{1}{(1 - e^{-j2\pi k/N_s})(1 - e^{j2\pi(k+r)/N_s})} \end{aligned} \tag{31}$$

where $d \in [-D, D]$. Note that there are singularity points when $d = 0$ or $d = -r$ in Equation (31), and the autocorrelation function become unavailable. For the first case ($d = -r$ and $d \neq 0$), let $d = -d$ and $r = -r$ to avoid the singularity point. For the second case ($d = 0$), thanks to the Hermitian symmetric property of the autocorrelation function, the value of the singularity point can be obtained by setting $r = 0$ and $d = r$. For the third case ($d = 0$ and $r = 0$), $\mathbb{E}\{h_f(0, k) h_f^*(0, k)\} = \frac{E_s - \sigma_{c0}^2}{E_s}$. Additionally, the autocorrelation function of ICI can be obtained by [19]:

$$\mathbb{E}\{c_{k-q,k} c_{k-q+r,k}^*\} \approx 4\pi^2 T_{sa}^2 \gamma(Q, r, N_s) \sum_{l=0}^{N_h-1} \sigma_l^2 \sigma_{Dl}^2 \tag{32}$$

where:

$$\gamma(D, r, N_s) = \sum_{\substack{m \notin [-D+q, D+q] \\ \cup [-D-r+q, D-r+q]}} \frac{1}{(1 - e^{-j2\pi(k-q)/N_s})(1 - e^{j2\pi(k+r-q)/N_s})}, \tag{33}$$

and the quantity $q = d - k$ denotes the subcarrier offset index.

Further simplification of Equation (33) can be obtained with some modifications as in [19]. It can be expressed as:

$$\gamma(D, r, N_s) = \gamma_0(D, r, N_s) - \gamma_1(D, r, N_s), \tag{34}$$

where:

$$\gamma_0(D, r, N_s) = \begin{cases} \frac{N_s^2}{12}, & r - q = 0, \\ \frac{N_s^2}{2\pi^2(r - q)^2}, & r - q \neq 0, \end{cases} \tag{35}$$

and:

$$\gamma_1(D, r, N_s) = \sum_{\substack{k \in [-D+q, D+q] \\ \cup [-D-r+q, D-r+q] \\ \setminus \{0, q-r\}}} \frac{N_s^2}{4\pi^2 k(k+r-q)} \tag{36}$$

Hence, the autocorrelation matrix $\mathbb{E}\{\mathbf{h}_k \mathbf{h}_k^H\}$ and $\mathbb{E}\{\mathbf{c}_k \mathbf{c}_k^H\}$ can be computed with the aid of Equations (31) and (32), respectively. The analytical pre-processing SINR ($\text{SINR}_Q^{(b)}$) and post-processing SINR after the matched filter ($\text{PSINR}_Q^{(b)}$) can be calculated by Equations (29) and (30).

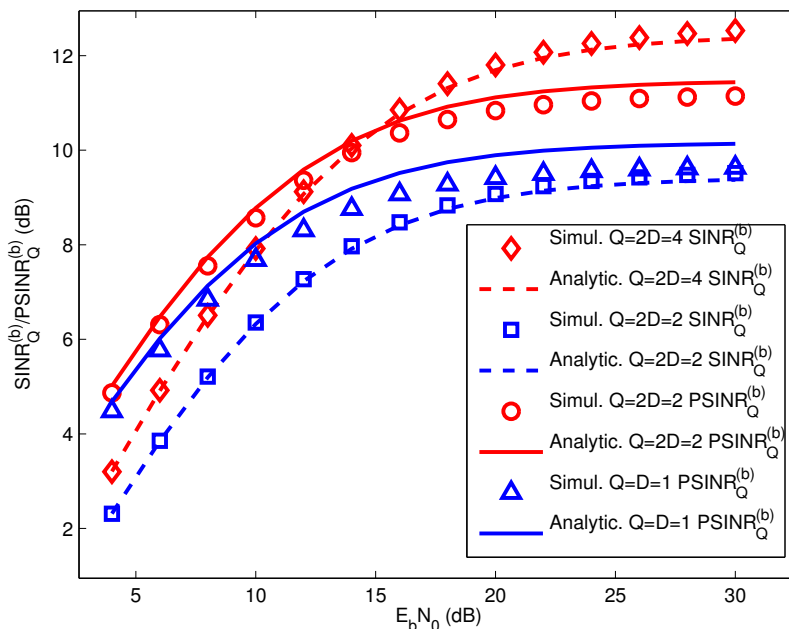


Figure 3. Pre-processing and post-processing signal-to-interference-plus-noise-ratio (SINR) comparison for the b -th feedback with different Q . $N_s = 128$, $f_d T_{\text{OFDM}} = 0.65$.

In the following, we present some simple numerical results and analytical results of pre-processing SINR ($\text{SINR}_Q^{(b)}$) and post-processing SINR ($\text{PSINR}_Q^{(b)}$) in Figure 3, and $f_d T_{\text{OFDM}} = 0.65$. We can observe that the post-processing SINR ($\text{PSINR}_Q^{(b)}$), with the same size Q , can be improved by the matched filter compared to pre-processing SINR ($\text{SINR}_Q^{(b)}$) at low SNR values. Furthermore, the post-processing SINR

performance gap between $Q = D = 1$ and $Q = 2D = 2$ is small (around 1 dB at 12 dB SNR). We can conjecture that the error probability of $\Pr(s_k^{(b)} \neq s_k)$, with $Q = D$ in Equation (10), will not be significantly degraded compared to that with $Q = 2D$. In other words, the multi-feedback cancellation with $Q = D$ requires less complexity than that with $Q = 2D$ in the cancellation stage, but achieves similar post-processing SINR performance.

6. BER Analysis of OFDM Systems with Residual ICI

First, the system model in Equation (2) needs to be rewritten in the following form without the ICI presence for the l -th path of the time-varying channels:

$$r_k(l) = \alpha_k(l)e^{j\theta_k(l)}s_k + v_k(l), \tag{37}$$

where $h_k(l) = \sum_{n=0}^{N_s-1} h_{kl}(n, l)e^{-j2\pi nk/N_s}$, the random variable (r.v.) $\alpha_k(l) = |h(k, l)|$ is the random channel gain for the l -th path at the n -th time slot, which follows the Rayleigh fading with the zero mean value and the variance σ_α^2 , and $\theta_k(l) = \arctan \frac{\Im(h_k(l))}{\Re(h_k(l))} \in [-\pi, \pi]$. The AWGN $v_l(n)$ denotes the same channel. Note that we assume that the interference inside the band is perfectly eliminated by the MBMF canceling strategy for simplicity. The received signal for the k -th subcarrier can be given as:

$$r_k = \sum_{l=0}^{N_h-1} r_k(l)P_k(l) + \sum_{m=0, m \neq k}^{N_s-1} \sum_{l=0}^{N_h-1} r_{k-m}(l)P_k(l) + \sum_{l=0}^{N_h-1} v_k(l)P_k(l), \tag{38}$$

where $P_k(l) = e^{-j2\pi(k/N_s)l}$, and thus, the output signals of the match filter for the decision variable can be given by:

$$\begin{aligned} \hat{s}_k &= s_k \underbrace{\sum_{q=-Q}^Q \sum_{l=0}^{N_h-1} \alpha_{k-q}^2(l)P_{k-q}^2(l)}_{\text{desired signal}} + \underbrace{\sum_{\substack{m=0, \\ m \notin [k-D+q, k+D+q]}}^{N_s-1} \sum_{q=-Q}^Q \sum_{l=0}^{N_h-1} \alpha_{k-q}(l)e^{j\theta_{k-q}(l)} \alpha_{k-m}(l)e^{j\theta_{k-m}(l)} P_k(l) s_m}_{\text{ICI}} \\ &+ \underbrace{\sum_{l=0}^{N_h-1} \alpha_k(l)e^{j\theta_k(l)} v_k(l)P_k(l)}_{\text{noise}} \\ &= s_k \sum_{q=-Q}^Q \sum_{l=0}^{N_h-1} \alpha_{k-q}^2(l)P_{k-q}^2(l) + \sum_{l=0}^{N_h-1} \sum_{q=-Q}^Q \alpha_{k-q}(l)e^{j\theta_{k-q}(l)} c_{k-q}(l) + v_k. \end{aligned} \tag{39}$$

From the equation above, we can observe that the PDF of the SINR becomes very non-trivial due to the superposition of desired signals and ICI from multiple subcarriers. If the channels vary rapidly in the time domain and the number of subcarriers becomes very large, the power of the desired signal ($q \neq 0$) from the adjacent subcarrier will become very close to that from the center subcarrier ($q = 0$) [4]. Thus, it is possible to approximate Equation (39) in another form:

$$\hat{s}_k \approx s_k(2Q + 1) \sum_{l=0}^{N_h-1} \alpha_k^2(l)P_k^2(l) + (2Q + 1) \sum_{l=0}^{N_h-1} \alpha_k(l) \sum_{q=-Q}^Q e^{j\theta_{k-q}(l)} c_{k-q}(l) + v_k, \tag{40}$$

To obtain the PDF of the SINR with the aid of Equations (32) and (33), the mathematical expression of SINR can be written as [29]:

$$\xi_k = \frac{\frac{E_s}{\sigma_v^2} (\sum_{l=0}^{N_h-1} \alpha_k^2(l))^2}{\frac{1}{2Q+1} \sum_{l=0}^{N_h-1} \alpha_k^2(l) + \frac{E_s}{\sigma_v^2} \sum_{l=0}^{N_h-1} \alpha_k^2(l) \sum_{q=-Q}^Q e^{j\theta_k(l)} \mathbb{E}(c_k(l)c_{k-q}^*(l)) e^{-j\theta_{k-q}(l)}}, \tag{41}$$

where:

$$\mathbb{E}(c_k(l)c_{k-q}^*(l)) = \sigma_{Dl}^2 \sigma_l^2 \underbrace{\sum_{\substack{m \notin [-D+q, D+q] \\ \cup [-D-r+q, D-r+q]}} \frac{1}{(1 - e^{-j2\pi(k-q)/N_s})(1 - e^{j2\pi(k+r-q)/N_s})}}_{\beta_l} \tag{42}$$

In order to further simplify the analysis, the normalized Doppler frequencies and the power are the same for any channel tap. The quantity β_l is a constant for any l . The Equation (41) becomes:

$$\begin{aligned} \xi_k &\approx \frac{\frac{E_s}{\sigma_v^2} (\sum_{l=0}^{N_h-1} \alpha_k^2(l))^2}{\frac{1}{2Q+1} \sum_{l=0}^{N_h-1} \alpha_k^2(l) + \beta_l \frac{E_s}{\sigma_v^2} \sum_{l=0}^{N_h-1} \alpha_k^2(l)} \\ &= \frac{\frac{E_s}{\sigma_v^2} (\sum_{l=0}^{N_h-1} \alpha_k^2(l))^2}{\frac{1}{2Q+1} \sum_{l=0}^{N_h-1} \alpha_k^2(l) + \beta_l \frac{E_s}{\sigma_v^2} \sum_{l=0}^{N_h-1} \alpha_k^2(l)} \end{aligned} \tag{43}$$

According to [30], the PDF of $X_k = \sum_{l=0}^{N_h-1} \alpha_k^2(l)$ can be expressed as:

$$f_X(x) = \frac{\zeta x^{L-1} e^{-\zeta x/\epsilon}}{(L-1)! \epsilon^L}, \tag{44}$$

where $\epsilon = 2\sigma_\alpha^2 b$, and the quantity σ_α^2 denotes the variance of $\alpha_k(l)$. We define $a = \frac{1}{2Q+1}$, $b = \frac{E_s}{\sigma_v^2}$ and $\zeta = \beta_l \frac{E_s}{\sigma_v^2}$. Additionally, Equation (43) is rewritten as:

$$\xi = \frac{bx}{a + \zeta x}, \tag{45}$$

$$x = \frac{\xi a}{b - \xi \zeta}, \tag{46}$$

$$\frac{d\xi}{dx} = \frac{ab}{(a + \zeta x)^2} = \frac{(\xi \zeta - b)^2}{ab} \tag{47}$$

Hence, the PDF of the SINR ξ can be expressed as [30]:

$$\begin{aligned} f_\xi(y) &= \frac{1}{|\frac{d\xi}{dx}|} f_X\left(\frac{ya}{b - y\zeta}\right) = \frac{ab}{(b - y\zeta)^2} f_X\left(\frac{ya}{b - y\zeta}\right) \\ &= \frac{ab}{(b - y\zeta)^2} \frac{\left[\left(\frac{ya}{b - y\zeta}\right)^{L-1} e^{\frac{ya}{(b - y\zeta)\epsilon}}\right]}{(L-1)! \epsilon^L} \\ &= \frac{ab(ya)^{L-1}}{(b - y\zeta)^{L+1}} \frac{e^{\frac{ya}{2(b - y\zeta)\sigma_\alpha^2 b}}}{(L-1)! (2\sigma_\alpha^2 b)^L} \end{aligned} \tag{48}$$

For the BER analysis of binary phase shift keying (BPSK) modulation, the conditional BER given the SINR ξ is given by [31]:

$$P_e(y) = Q(\sqrt{2y}), \tag{49}$$

where the notation $Q(\cdot)$ denotes the Q-function for the error probability calculation. The average BER can be given as:

$$\bar{P}_e = \int_0^{+\infty} Q(\sqrt{2y}) f_\xi(y) dy, \tag{50}$$

For the numerical evaluation of Equation (50), the average BER needs to be decomposed as follows:

$$\begin{aligned} \bar{P}_e &= \int_0^{+\infty} \frac{1}{2} f_\xi(y) dy - \int_0^{+\infty} \frac{1}{2} \phi(\sqrt{y}) f_\xi(y) dy \\ &= \frac{1}{2} \int_0^{+\infty} y^0 f_\xi(y) dy - \frac{1}{\sqrt{\pi}} \sum_{i=1}^{+\infty} \frac{(-1)^{i+1}}{(2i-1)(i-1)!} \int_0^{+\infty} y^{\frac{2i-1}{2}} f_\xi(y) dy \end{aligned} \tag{51}$$

where $\phi(x) = \frac{2}{\sqrt{\pi}} \sum_{i=1}^{+\infty} \frac{(-1)^{i+1}}{(2i-1)(i-1)!} x^{2i-1}$ as in [32]. According to [29], we can obtain the following equation:

$$\int_0^{+\infty} y^i f_\xi(y) dy = \frac{(\frac{b\epsilon}{a})^i}{(L-1)!} \int_0^{-1/\zeta\epsilon} \frac{x^{L+i-1}}{(1 + \frac{\zeta\epsilon}{a}x)^i} e^{-x} dx, \tag{52}$$

where:

$$\int_0^{-1/\zeta\epsilon} \frac{x^{L+i-1}}{(1 + \frac{\zeta\epsilon}{a}x)^i} e^{-x} dx = \frac{a^i}{(-\frac{\zeta\epsilon}{a})^{L+i} \Gamma(i)} \sum_{j,k=0}^{+\infty} \frac{\Gamma(i+j)}{L+i+j+k} \frac{(\frac{\zeta\epsilon}{a})^{-j}}{j!k!} \tag{53}$$

and $\Gamma(t) = \int_0^\infty x^{t-1} e^{-x} dx$ denotes the Gamma function. Hence, the average BER can be obtained by Equation (50) with Equations (52) and (53). The analytical result of the uncoded BER with different band widths $Q=2, 4, 6$ is plotted in Figure 4, with $f_d T_{\text{OFDM}} = 0.65$ the uniform power delay profile $L = 8$ (β_l is a constant for any l). It can be observed that the analytical curves are approximately in agreement with the simulated ones, but the curves with $Q > 6$ are not plotted due to the significant mismatch to the simulated ones. This is because more interference is removed from the desired signals that cause the inaccuracy of the autocorrelation function of the ICI approximation in Equation (42), the PDF of which does not follow the similar distribution as described in Equation (44). Although the mismatch exists in the analysis, the analysis will be more reliable in the low Doppler frequency scenarios with small band sizes Q .

7. SINR Ordering for MBMF-SIC

For conventional sequential ICI cancellation for OFDM systems, the cancellation is performed on a subcarrier by subcarrier basis, because the previous soft symbol estimates $[\hat{s}_{k-2D}, \dots, \hat{s}_{k-1}]$ inside the band are needed in the cancellation for the desired subcarrier s_k . In this case, there is no significant benefit from the ordering, due to the absence of previous soft symbol estimates. With the iterative ICI cancellation and the channel decoder, the soft symbol estimates $[\hat{s}_{k-2D}, \dots, \hat{s}_{k-1}]$ are known beyond the initial iteration, so any ordering can be performed. However, its performance improvement by ordering is very small. On the other hand, the sequential ICI cancellation will introduce the aggregation of

residual interference. For MBMF-SIC, the interference is reconstructed by the multi-feedback symbols vectors $[s_{k-2D}^b, \dots, s_{k-1}^b]$, $b = 1, 2, \dots, B$, so the aggregation of residual interference from previous soft symbols can be significantly removed. Furthermore, we assume that the conditional probabilities of $\mathbf{y}_k^{(b)}$ given $\mathbf{s}_k^{(b)}$ and $\tilde{\mathbf{y}}_k$ given $\hat{\mathbf{s}}_{\bar{k}}$ are conditionally independent in Equation (15). This will be true if the residual interference inside the band in Equations (10) and (12) dominates. This assumption may be more reasonable by the ordering, which can reduce the coupling effects brought by the previous soft symbol estimates. Following Equations (10) and (30), the SINR of the k -th subcarrier for ordering can be evaluated as similar to the SINR ordering for the conventional SIC.

$$\nu_k \approx \frac{(|\mathbf{h}_k^H \mathbf{h}_k|)^2 E_s}{E_s \text{tr}(\mathbb{E}\{\mathbf{h}_k \mathbf{h}_k^H\} \mathbb{E}\{\mathbf{c}_k \mathbf{c}_k^H\}) + \sigma_v^2 + \text{tr}(\sum_{\bar{k}=k-Q, q \neq k}^{k+Q} \mathbf{h}_{\bar{k}} \nu_{\bar{k}} \mathbf{h}_{\bar{k}}^H)}, \tag{54}$$

where $\nu_k = \mathbb{E}\{(s_q - \hat{s}_q)(s_q - \hat{s}_q)^*\}$. In the remaining steps, the quantity ν_k can be sorted for $k = 1, \dots, N_s$, and the detection ordering can be implemented accordingly. Other ordering methods can also be employed on the basis of the error probability or LLRs, the calculation of which will introduce the channel matrix inversion, with complexity at least $\mathcal{O}((2D + 1)^2)$. Hence, the complexity of LLR ordering in [33] will be more complicated than that of SINR ordering.

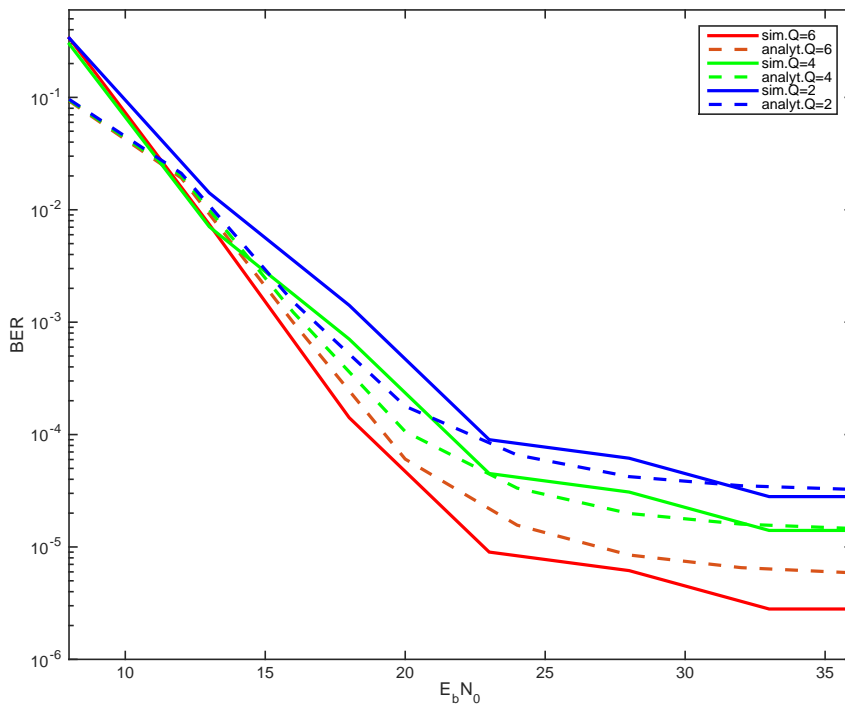


Figure 4. The uncoded bit error rate analysis of the system with the presence of the residual inter-carrier interference (ICI) outside the band ($Q = 2,4,6$). $N_s = 128$, $f_d T_{\text{OFDM}} = 0.65$, $L = 8$.

8. Multi-Segmental Channel Estimation

In this section, we present the MSCE technique to estimate time-varying channels and discuss the pilot symbol selection in each iteration. Additionally, the MSCE can be terminated in an early iteration by comparing with previous estimates.

8.1. Least-Squares-Based MSCE

For MSCE, we split the received signal $r_n, n = 0, 1, \dots, N_s - 1$ into T segments, and each segment has $M = N_s/T$ samples. The FFT can be performed partially as expressed as follows:

$$\begin{aligned}
 y_t(d) &= \frac{1}{\sqrt{N_s}} \sum_{n=(t-1)N_t}^{tN_t-1} r_n e^{-j\frac{2\pi}{N_s}dn} \\
 &= \frac{1}{N_s} \sum_{n=(t-1)N_t}^{tN_t-1} \sum_{l=0}^{N_h-1} h_{tl}(n, l) e^{-j\frac{2\pi}{N_s}kl} \cdot \sum_{k=0}^{N_s-1} s_k e^{-j\frac{2\pi}{N_s}nk} e^{-j\frac{2\pi}{N_s}nd} \\
 &= \frac{1}{N_s} \sum_{k=0}^{N_s-1} s_k \sum_{n=(t-1)N_t}^{tN_t-1} h_f(n, k) e^{-j\frac{2\pi}{N_s}n(d-k)}
 \end{aligned} \tag{55}$$

where the quantity $h_f(n, k)$ denotes the channel frequency response for the k -th subcarrier at time index n . We assume that the channel remains constant during segment t , so Equation (55) can be simplified as [7]:

$$\begin{aligned}
 y_t(d) &= \sum_{k=0}^{N_s-1} s_k h_f(t, k) \frac{1}{N_s} \sum_{n=(t-1)N_t}^{tN_t-1} e^{-j\frac{2\pi}{N_s}n(d-k)} \\
 &= \sum_{k=0}^{N_s-1} s_k h_f(t, k) \delta_t(d - k),
 \end{aligned} \tag{56}$$

where:

$$\delta_t(d - k) = \frac{1}{T} e^{j2\pi(d-k)\frac{2t-1}{2T}} \text{sinc}\left(\frac{\pi(d - k)}{T}\right). \tag{57}$$

By defining $\mathbf{y}_t = [y_t(0), \dots, y_t(N_s - 1)]^T$, $\mathbf{h}_{df}(t) = [h_{df}(t, 0), \dots, h_{df}(t, N_s - 1)]^T$, $\mathbf{h}_{tl}(t) = [h_{tl}(t, 0), \dots, h_{tl}(t, l), \dots, h_{tl}(t, L - 1)]^T$, and the term $\delta_k(t)$ in Equation (57) is re-organized in a matrix form as:

$$\Delta_t = \begin{bmatrix} \delta_0(t) & \dots & \delta_{N_s-1}(t) \\ \vdots & \ddots & \vdots \\ \delta_{1-N_s}(t) & \dots & \delta_0(t) \end{bmatrix}, \tag{58}$$

Equation (55) for the t -th segment can be rewritten in the following form:

$$\mathbf{y}_t = \underbrace{\sqrt{N_s} \Delta_t \text{diag}(\mathbf{s}) \mathbf{F}_L}_{\mathbf{A}} \mathbf{h}_{tl}(t), \tag{59}$$

where $\mathbf{h}_{df}(t) = \sqrt{N_s} \mathbf{F}_L \mathbf{h}_{tl}(t)$. Using LS estimation in the time domain [26], the channel estimates in the t -th segment can be obtained by:

$$\hat{\mathbf{h}}_{tl}(t) = (\mathbf{A}^H \mathbf{A})^{-1} \mathbf{A}^H \mathbf{y}_t. \tag{60}$$

Note that there are N_p pilot symbols already known to the receiver, and the zeroes can be set for the unreliable symbol estimates of $\hat{\mathbf{s}}$ in each iteration, the reliability of which can be evaluated by LLRs from

the channel decoder. In the following steps, we introduce the piece-wise linear model to approximate the channel impulse responses for the time-varying channels between the t -th segment and $(t + 1)$ -th segment, as in [34]. Hence, the channel estimates $\hat{\mathbf{h}}_{tl}(n) = [\hat{h}_{tl}(n, 0), \dots, \hat{h}_{tl}(n, l), \dots, \hat{h}_{tl}(n, L - 1)]^T$ for different time indices can be obtained, and the corresponding channel frequency response $\hat{h}_{df}(d, k)$ can be obtained. The matrix $\mathbf{\Delta}_t$ can be pre-computed, once the number of segments T is determined. In addition, the differences of channel estimates between the $(p - 1)$ -th and p -th iteration can be measured, which can help us to terminate the MSCE at an earlier iteration.

8.2. MSE Lower Bound Analysis

In this subsection, we derive an overall MSE lower bound as a benchmark for the MSCE discussed above. As can be seen from above, the MSCE exploits the linear interpolation to approximate the channels between segments, that is an error approximation in the channel estimates rather than the noise itself. Firstly, the channel estimates after the interpolation can be rewritten in another form as:

$$\tilde{\mathbf{h}}_{tl} = \mathbf{\Phi} \hat{\mathbf{c}} \tag{61}$$

where:

$$\begin{aligned} \tilde{\mathbf{h}}_{tl} &= [\tilde{\mathbf{h}}_{tl}^T(0), \dots, \tilde{\mathbf{h}}_{tl}^T(l), \dots, \tilde{\mathbf{h}}_{tl}^T(L - 1)]^T \in \mathbb{C}^{N_s L \times 1}, \\ \tilde{\mathbf{h}}_{tl}(l) &= [\tilde{h}_{tl}(0), \dots, \tilde{h}_{tl}(n), \dots, \tilde{h}_{tl}(N_s - 1)]^T \in \mathbb{C}^{N_s \times 1}, \\ \hat{\mathbf{c}} &= [\hat{\mathbf{h}}_{tl}^T(0), \dots, \hat{\mathbf{h}}_{tl}^T(l), \dots, \hat{\mathbf{h}}_{tl}^T(L - 1)] \in \mathbb{C}^{TL \times 1} \\ \hat{\mathbf{h}}_{tl}(l) &= [\hat{h}_{tl}(0, l), \dots, \hat{h}_{tl}(t, l), \dots, \hat{h}_{tl}(T - 1, l)]^T, \end{aligned} \tag{62}$$

and:

$$\begin{aligned} \mathbf{\Phi} &= \mathbf{I}_L \otimes \mathbf{\Psi}, \\ \mathbf{\Psi} &= [\boldsymbol{\psi}(0), \dots, \boldsymbol{\psi}(n), \dots, \boldsymbol{\psi}(N_s - 1)]^T \in \mathbb{R}^{N_s \times T} \\ \boldsymbol{\psi}(n) &= [\psi(n, 0), \dots, \psi(n, q), \dots, \psi(n, T - 1)]^T \end{aligned} \tag{63}$$

where $\psi(n, q)$ denotes the interpolation coefficients. Defining the noise term and the residual interference term in as \mathbf{z}_t , Equation (59) can be rewritten in a compact matrix form:

$$\begin{aligned} \mathbf{y} &= \underbrace{\begin{bmatrix} \mathbf{\Lambda}_0 & & \\ & \ddots & \\ & & \mathbf{\Lambda}_{T-1} \end{bmatrix}}_{\boldsymbol{\theta} \in TN_s \times TN_s} \underbrace{\begin{bmatrix} \mathbf{F}^H & & \\ & \ddots & \\ & & \mathbf{F}^H \end{bmatrix}}_{\mathbf{F}' \in TN_s \times TN_s} \underbrace{\begin{bmatrix} \text{diag}(\mathbf{s}) \\ \vdots \\ \text{diag}(\mathbf{s}) \end{bmatrix}}_{\mathbf{S} \in TN_s \times N_s} \mathbf{\Gamma} \mathbf{\Phi} \mathbf{c} \\ &+ \underbrace{\begin{bmatrix} \mathbf{z}_0 \\ \vdots \\ \mathbf{z}_{T-1} \end{bmatrix}}_{\mathbf{z} \in TN_s \times 1} \end{aligned} \tag{64}$$

where:

$$\begin{aligned} \mathbf{F} &= [\mathbf{\Lambda}_0, \dots, \mathbf{\Lambda}_t, \dots, \mathbf{\Lambda}_{T-1}] \in \mathbb{C}^{N_s \times N_s} \\ \mathbf{y} &= [\mathbf{y}_0^T, \dots, \mathbf{y}_t^T, \dots, \mathbf{y}_{T-1}^T]^T \in \mathbb{C}^{TN_s \times 1} \\ \mathbf{\Gamma} &= [\boldsymbol{\gamma}_0^T, \dots, \boldsymbol{\gamma}_k^T, \dots, \boldsymbol{\gamma}_{N_s-1}^T] \in \mathbb{C}^{N_s \times N_s L} \end{aligned} \tag{65}$$

and:

$$\begin{aligned} \Lambda_t &\in \mathbb{C}^{N_s \times M}, \\ \gamma_k &= \underbrace{[0, \dots, 0]_{k+1}}_{k+1} e^{-j \frac{2\pi}{N_s} k \cdot 0}, \underbrace{[0, \dots, 0]_{LN_s}}_{LN_s} e^{-j \frac{2\pi}{N_s} k l}, \underbrace{[0, \dots, 0]_{(L-l)N_s}}_{(L-l)N_s} e^{-j \frac{2\pi}{N_s} k(L-1)}, \\ \underbrace{[0, \dots, 0]_{N_s-k+1}}_{N_s-k+1} &]^T \in \mathbb{C}^{LN_s \times 1}, \end{aligned} \quad (66)$$

Hence, Equation (64) can be represented as:

$$\mathbf{y} = \underbrace{\Theta \mathbf{F}' \mathbf{S} \mathbf{\Gamma} \mathbf{\Phi}}_{\mathbf{B}} \mathbf{c} + \mathbf{z}, \quad (67)$$

where the matrix θ denotes the partial FFT and the matrix \mathbf{F}' denotes the standard IFFT. The channel estimates $\hat{\mathbf{c}} = \hat{\mathbf{h}}_{tl}$ can be obtained by LS estimation accordingly. The overall MSE is based on the approximation errors of linear interpolation and the estimation error of $\hat{\mathbf{c}}$, namely MSE_{approx} and MSE_{est} , respectively. According to the derivation of [35], the overall MSE can be expressed as:

$$\text{MSE}_{overall} = \text{MSE}_{approx} + \text{MSE}_{est}. \quad (68)$$

where:

$$\begin{aligned} \text{MSE}_{approx} &= \frac{1}{N_s L} \text{tr}\{(\mathbf{I}_{N_s} - \mathbf{\Psi} \mathbf{\Psi}^H) \mathbf{R}\} \\ \text{MSE}_{est} &= \frac{1}{N_s L} \text{tr}\{\mathbb{E}((\mathbf{c} - \hat{\mathbf{c}})(\mathbf{c} - \hat{\mathbf{c}})^H)\} \end{aligned} \quad (69)$$

Note that the unity power of the multipath channel is assumed. Thus, $\mathbb{E}(\mathbf{h}_{tl}^H \mathbf{h}_{tl}) = 1$. Additionally, the matrix \mathbf{R} represents the autocorrelation matrix of the channels in the time domain. The autocorrelation matrix of $\mathbb{E}((\mathbf{c} - \hat{\mathbf{c}})(\mathbf{c} - \hat{\mathbf{c}})^H)$ can be given by:

$$\mathbb{E}((\mathbf{c} - \hat{\mathbf{c}})(\mathbf{c} - \hat{\mathbf{c}})^H) = \mathbb{E}(\mathbf{z} \mathbf{z}^H) \mathbb{E}(\mathbf{B} \mathbf{B}^H) \quad (70)$$

where the cross-correlation function of noise is $\mathbb{E}\{z_t(d_1) z_t(d_2)\} = \frac{\sigma_v^2}{T} e^{-j \frac{\pi(d_1-d_2)(2t-1)}{T}} \text{sinc}(\frac{\pi(d_1-d_2)}{2T})$, and the notation sinc denotes the sinc function. Because we assume all data and pilot symbols for transmission are known to the channel estimator in the later iterations, this means that the matrix \mathbf{B} can be calculated and $\mathbb{E}(\mathbf{B} \mathbf{B}^H)$ accordingly. The overall MSE lower bound is given by:

$$\text{MSE}_{overall} = \frac{1}{N_s L} \text{tr}\{(\mathbf{I}_{N_s} - \mathbf{\Psi} \mathbf{\Psi}^H) \mathbf{R}\} + \frac{1}{N_s L} \text{tr}\{\mathbb{E}(\mathbf{z} \mathbf{z}^H) \mathbb{E}(\mathbf{B} \mathbf{B}^H)\} \quad (71)$$

Note that the prior assumption that channels are constant within the segment is not used in the MSE analysis, so the overall MSE is a lower bound for MSCE.

9. Complexity Requirements of MBMF-SIC and MSCE

The complexity of the MBMF-SIC discussed in this chapter is determined by the following parameters: the number of multi-feedback candidates B , the reduced size truncated channel matrix $Q = D$, the number of subcarriers N_s and the number of iterations for the cancellation P . Following the description of the algorithm in Algorithm 1 with QPSK, the computation of the algorithm for the initial

iteration is slightly different from that for the later iterations. However, the computational complexity of the initial iteration is almost identical to that of the later iterations. This is because the initial LLRs first need to be calculated by the output of the matched filter, rather than the direct use of the output of the channel decoder. The computational complexity comes from two aspects: (1) the multi-feedback generation; and (2) the multi-feedback cancellation. The computation of feedback symbols generation for $k = 0, 1, \dots, N_s - 1$ in Step 11 requires a maximum of $8N_sBD$ complex additions (CAs) for GSG and TSG, and the computation of the cancellation in Steps 12 and 13 for $k = 0, 1, \dots, N_s - 1$ requires $N_sB(8D^2 + 6D + 1)$ complex multiplications (CMs) and $N_sB(8D^2 + 6D + 2)$ CAs. In Step 14, the computation of average probability of $\Pr(s_k(i) = +1|\mathbf{y}_k^*), i = 1, 2$ and $k = 0, 1, \dots, N_s - 1$ and the corresponding LLR leads to N_sB CAs. Hence, the total number of complex operations for one iteration required by the MFMB-SIC is $N_s(16BD^2 + 20BD + 4B)$, and the SINR ordering requires a total of $\mathcal{O}(N_s \log N_s) + N_s$ complex operations [14]. The complexity comparison of ICI cancellation techniques has been made in Table 1. The complexity of MBMF-SIC and MF-PIC is moderate compared to MF-SIC and much lower than that of conventional MMSE-SIC and banded MMSE-SIC.

Furthermore, the MSCE requires a maximum of $\mathcal{O}(TL^2) + \mathcal{O}(2N_sL)$ complex operations for each OFDM symbol in the p -th iteration. This is because the size of the matrix inversion used in Equation (60) is only related to the number of channel paths L . The complexity comparison between different channel estimation techniques for rapidly time-varying channels is presented in Table 2. Note that pilot-assisted LS denotes the pilot-assisted LS channel estimation, which uses the discrete Karhuen–Loève basis expansion model (BEM) to approximate the time-varying channels with the limited number of expansion coefficients [36]. The number of expansion coefficients is lower bounded by $2\lceil f_d T_{\text{OFDM}} \rceil + 1 = 2D - 1$ as described in [35]. The significant advantage of MSCE over the method in [36] is the use of linear interpolation to approximate the channels between two segments in the OFDM symbol. Hence, the MSCE can be considered as a special representation of BEM with two expansion coefficients. Compared to SBCE, the complexity of MSCE is a bit higher; because the matrix inversion with the size L is required to estimate the channels in the mid-point of each segment.

Table 1. Complexity comparison between different interference cancellation techniques for the p -th iteration. BP, belief propagation; RSL, recursive-SIC-linear-MMSE.

Algorithm	Complex Operations
MMSE-SIC [37]	$\mathcal{O}(N_s^3) + \mathcal{O}(4N_s^2D^2) + \mathcal{O}(N_s^2)$
banded MMSE-SIC [4]	$N_s(\frac{64}{3}D^3 + 80D^2 + \frac{104}{3}D + 4)$
MF-SIC [16]	$N_s(32D^2 + 16D + 3)$
MF-PIC [17]	$N_s(32D^2 + 22D + 1)$
RSL [3]	$N_s(28D^3 + 60D^2)$
BP-MAP [15]	$\mathcal{O}(N_s C ^{2D+1})$ * $ C $ denotes the number of constellation points
MBMF-SIC	$N_s(16BD^2 + 20BD + 4B)$
MBMF-SIC + SINR ordering	$N_s(16BD^2 + 20BD + 4B) + \mathcal{O}(N_s \log N_s) + N_s$

Table 2. Complexity comparison between different channel estimation techniques for the p -th iteration.

Algorithm	Complex Operations
SBCE [16]	$\mathcal{O}(N_s^2) + \mathcal{O}(2N_sL)$
PA-LS [36]	$\mathcal{O}((2D^2 - 1)L^3) + \mathcal{O}((4DN_s - 2)L^2)$
MSCE	$\mathcal{O}(TL^3) + \mathcal{O}(2N_sL)$

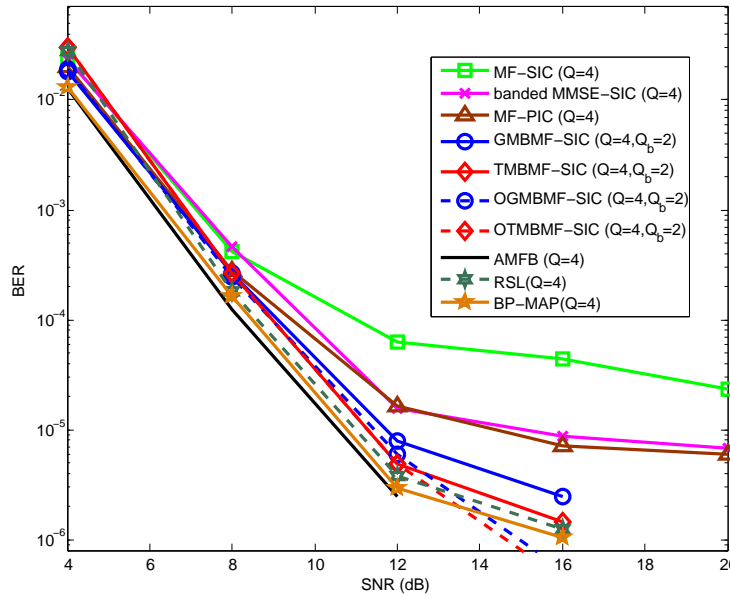


Figure 5. BER performance against SNR (dB) of MF-PIC, GSG-based MBMF-SIC, ordering GSG-based MBMF (OGMBMF)-SIC, TSG-based MBMF (TMBMF)-SIC, ordering TMBMF (OTMBMF)-SIC, MF-SIC, banded MMSE-SIC and approximate matched filter bound (AMFB) in the fourth iteration with $f_d T_{\text{OFDM}} = 0.65$.

10. Simulation Results

In this section, the performance of the proposed methods (MF-PIC and MBMF-SIC) will be evaluated in terms of BER in different scenarios. We assume a scenario with the following settings: the carrier frequency $f_c = 650$ MHz; the subcarrier spacing $\Delta f = 976.5$ Hz; and the OFDM symbol period is $T_{\text{OFDM}} = 1/\Delta f \approx 1$ ms. The number of subcarriers is $N_s = 128$. The symbols are modulated by QPSK, the extension of which to other modulation schemes is straightforward. In addition, a 1/2 rate convolutional code with generator polynomial (7, 5) is employed for the iterative interference cancellation, and the length of the code is 2560 bits. A wide-sense stationary uncorrelated scattering channel with a uniform power delay profile is simulated according to the Jakes model and the normalized Doppler frequency $f_d T_{\text{OFDM}} = 0.65$. The maximum delay of the channel is $L = 8$. Because of the band assumption, we assume $D = \lceil f_d T_{\text{OFDM}} \rceil + 1$ as described in [4,5] given the time-domain window. For MSCE, the number of segments $T = 2$ is used, and the number of pilots $N_p = N_s/4$. We also define an approximate matched filter bound (AMFB) [4] as a benchmark for ICI cancellation, which implies that the ICI inside the band ($Q = 2D$) is perfectly removed. Additionally, we use the banded

MMSE-SIC [4], MF-SIC [16] and MBMF-SIC with and without SINR ordering, as well as AMFB for comparison.

In Figure 5, we introduce several OFDM equalization techniques for comparison. The list includes the approximate MAP equalizers, namely belief propagation Ungerboeck-MAP (BP-MAP), recursive-SIC-linear-MMSE (RSL) in [3,15], the benchmark AMFB without ICI inside the band [2], the banded MMSE-SIC [4] and MF-SIC [16]. Note that the RSL we used is a modified SIC-MMSE with two taps ($Q = 4$) in the fourth iteration. The BER performance of GSG-based MBMF-SIC (GMBMF-SIC) and TSG-based MBMF-SIC (TMBMF-SIC) with SINR ordering show performances close to the approximate MAP equalizers (BP-MAP), with only 1 dB loss with the BP-MAP and a fraction of 1 dB loss with the benchmark AMFB. The proposed scheme may significantly reduce the error floor compared to banded MMSE-SIC and MBMF-SIC without SINR ordering. It can be seen that the SINR ordering improves the reliability of detected symbols and makes the assumption for Equation (14) more appropriate. For a fair comparison, the SINR ordering in Section 7 is incorporated in other schemes in the later iterations except for the first iteration. This is because serial ICI cancellation requires previous symbol estimates to improve the reliability of the remaining symbols. However, the ordering for MBMF-SIC can be employed in the initial iteration due to the use of LLR to generate multi-feedback candidates in the Steps 3 and 4 of Algorithm 1. We can also observe that the BER performance difference between GMBMF-SIC and TMBMF-SIC is negligible, but TSG performs better than GSG. This also agrees with the statements in [27] that the tree search algorithm works better than the Gibbs sampler at high SNR. For simplicity, we only consider GMBMF-SIC and TMBMF-SIC with SINR ordering in the rest of the chapter, which will be referred to as OGMBMF-SIC and OTMBMF-SIC. Furthermore, the curves of OTMBMF-SIC may not be shown in some following figures, because there is no significant difference between OGMBMF-SIC and OTMBMF-SIC in the BER performance. In what follows, the RSL is not plotted, due to its close to AMFB performance. Unlike the RSL, the BP-MAP may outperform other ICI cancellation methods. This is because the ICI cancelers mitigate the uncoded interference from neighbor subcarriers, but in the BP-MAP scheme, more reliable extrinsic information is obtained from the channel decoder in an iterative detection and decoding system. Hence, its performance will be improved by the additional weights when the LLR value is updated. However, the BP-MAP performs a little worse than the proposed MBMF-SIC with SINR ordering, which introduces additional precoding gain and removes the error floor.

The BER performance of the fourth iteration against normalized Doppler frequencies $f_d T_{\text{OFDM}}$ from 0.25 to 0.65 has been illustrated in Figure 6, which validates the statements that the proposed OGMBMF-SIC and OTMBMF-SIC can work in a wide range of high Doppler frequencies $f_d T_{\text{OFDM}}$. We can observe that the power of ICI inside the band is reduced at high Doppler frequencies. Additionally, the MF-SIC and MF-PIC can only be used at low Doppler frequencies.

Figure 7 compares the BER performance against SNR (dB) with a normalized Doppler frequency $f_d T_{\text{OFDM}} = 0.65$ in the fourth iteration. The MSCE is iteratively performed in every iteration, once the new symbol estimates become available from the channel decoder. The BER performance of these receivers in the first iteration is very poor, with $f_d T_{\text{OFDM}} = 0.65$, which may not be useful for comparison. Matched filter-based receivers (MF-SIC, OGMBMF-SIC) are less sensitive to channel estimation errors, because they do not make use of channel coefficients as much as banded MMSE-SIC. For banded

MMSE-SIC, the autocorrelation matrix must be used, which may amplify the channel estimation errors. In Figure 5, the banded MMSE-SIC outperforms MF-SIC with perfect channel knowledge in the BER performance. However, their performance at SNR = 20 dB has been degraded to the same level of BER (less than 1 dB performance loss) in the fourth iteration with MSCE. MF-PIC is not very close to banded MMSE-SIC with channel estimation, because the autocorrelation matrix is also required for MF-PIC for ICI cancellation. Intuitively, the proposed OGMBMF-SIC has the same advantages as MF-SIC. With MSCE, OGMBMF-SIC can still achieve an acceptable BER performance in such a high mobility scenario ($f_d T_{\text{OFDM}} = 0.65$), which makes OGMBMF-SIC more practical.

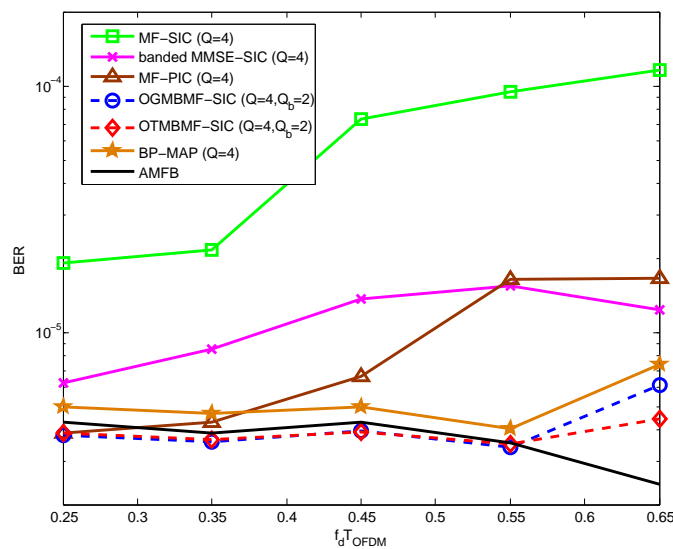


Figure 6. BER performance against $f_d T_{\text{OFDM}}$ of MF-PIC, OGMBMF-SIC, OTMBMF-SIC, MF-SIC and banded MMSE-SIC in the fourth iteration at SNR =12 dB.

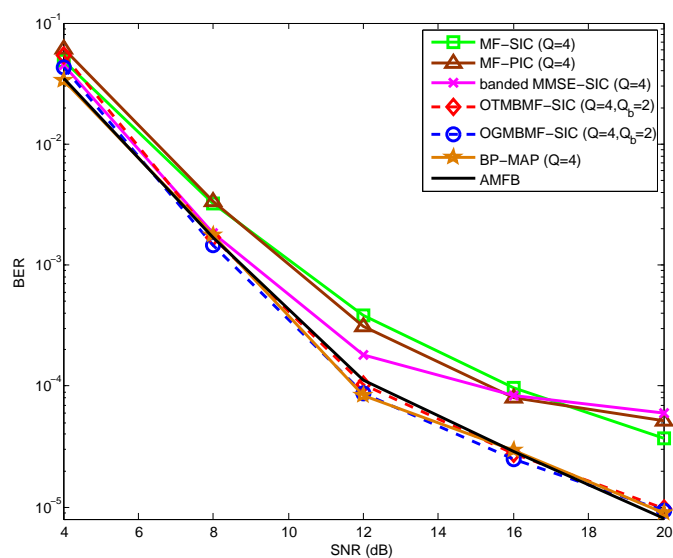


Figure 7. BER performance against SNR (dB) of MF-PIC, GMBMF-SIC, OGMBMF-SIC, MF-SIC, banded MMSE-SIC and AMFB using MSCE in the fourth iteration with $f_d T_{\text{OFDM}} = 0.65$.

To show the robustness to the high normalized Doppler frequencies, we compared the SBCE, PA-LS and MSCE in terms of BER performance in the fourth iteration. In Figure 8, the MF-PIC and OGMBMF-SIC with SBCE cannot work at normalized Doppler frequencies over 0.4. Additionally, the curves for MSCE are almost identical to those for PA-LS, only slightly poorer at high normalized Doppler frequencies, which implies that the MSCE performed in an iterative manner and with the aid of data symbols can approach the performance of PA-LS, which uses the discrete Karhunen-Loève (DKL)-basis expansion model (BEM) to approximate the channels with five expansion coefficients.

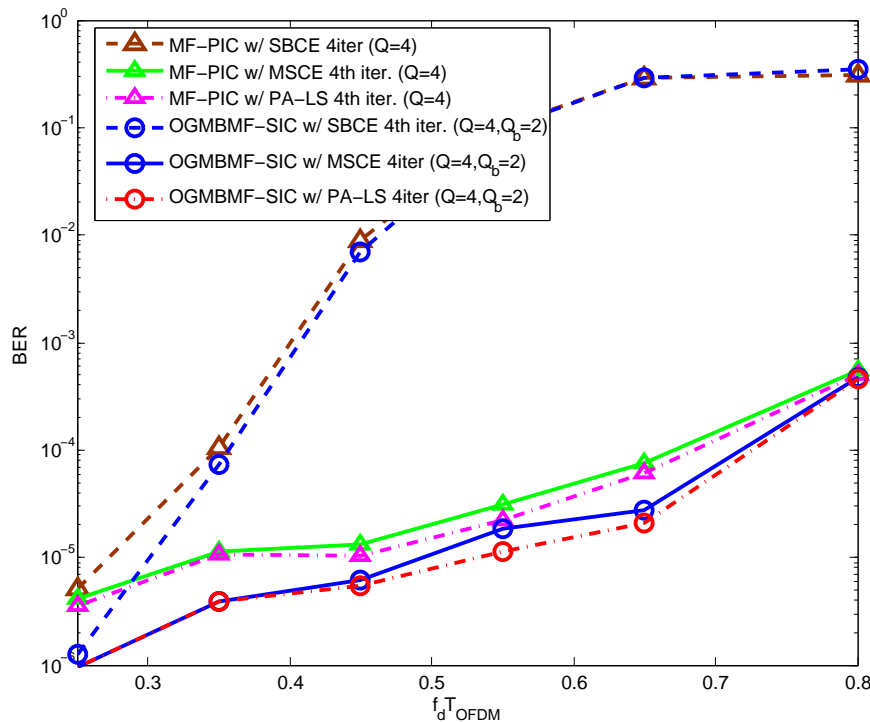


Figure 8. BER performance against $f_d T_{\text{OFDM}}$ of OGMBMF-SIC and MF-PIC using MSCE and single-burst channel estimation (SBCE) in the fourth iteration at SNR =16 dB.

To determine an appropriate number of multi-feedback candidates (B) of MBMF-SIC for a given normalized Doppler frequency, the BER performance against the number of feedback elements has been plotted in Figure 9 for OGMBMF-SIC and OTMBMF-SIC. The BER performance improves with an increasing number of feedback elements. We also observed that both of them reach the optimum BER performance around $B = 7$ in the fourth iteration, which implies that both generation mechanisms can be considered as equivalent, if more iterations are performed by the receivers. Unlike the BER performance of OTMBMF-SIC, the BER performance of OGMBMF-SIC is poorer than that of OTMBMF-SIC in the first several iterations. This is because the feedback of OGMBMF-SIC is randomly generated given the *a priori* probability from the output of the channel decoder, and we assume each of them has equal probability, which may introduce instability into the LLR calculation with the increasing number of feedback elements. For OTMBMF-SIC, each feedback candidate has been weighted given the probability, so the feedback elements with low probability will not have a significant influence on the BER performance. In other words, it only takes the most significant feedback candidates into account. Furthermore, MBMF-SIC is not equivalent to the MAP algorithm and employs the reduced channel

matrix in the multi-feedback cancellation. Thus, a large B does not significantly improve the BER performance as compared to a small B .

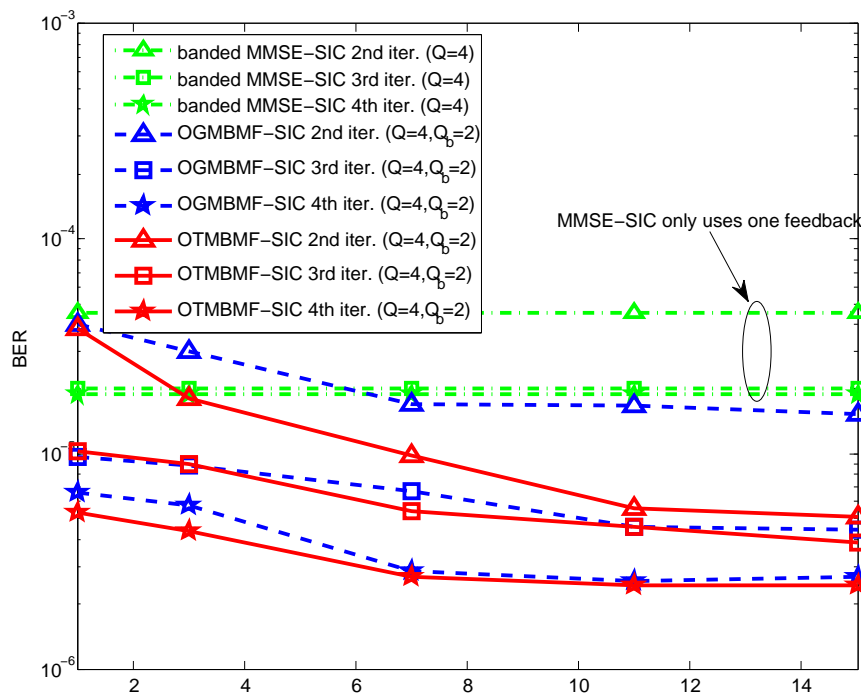


Figure 9. BER performance against the number of multi-feedback candidates B with $f_d T_{\text{OFDM}} = 0.65$ at SNR =12 dB.

11. Conclusions

In this paper, we have presented a novel multi-feedback matched filter (MBMF) strategy for coded iterative receivers for OFDM systems over rapidly time-varying channels. The proposed approach employs a multiple ICI cancellation strategy and approximates the residual interference inside the band by introducing multiple cancellation feedback candidates, which are generated by two different mechanisms: Gibbs sampling-based generation (GSG) and tree search-based generation (TSG). The BER performance of the proposed algorithm was analyzed, and the simulation results indicated that the proposed MBMF-PIC can achieve a close to Ungerboeck-MAP performance and outperforms other existing soft ICI cancellation techniques at the expense of a moderate complexity increase. For imperfect channels, the proposed MBMF-SIC can still achieve an acceptable BER performance at high normalized Doppler frequencies and provides an attractive tradeoff between performance and complexity.

Acknowledgments

This work is supported by the Scientific Research Foundation of Chengdu University of Information Technology (CUIT) (No. KYTZ201415), the Scientific Research Foundation for the Returned Overseas Chinese Scholars, State Education Ministry and the Sichuan Provincial Department of Science and Technology Innovation and R&D projects in Science and Technology Support Program

(No. 2015RZ0060). This work is also supported by the Startup Foundation for Introducing Talent of Nanjing University of Information Science & Technology (NUIST).

Author Contributions

Jiao Feng and Peng Li conceived and designed the experiments; Li (Alex) Li performed the experiments; Li (Alex) Li and Peng Li analyzed the data; Li (Alex) Li contributed reagents/materials/analysis tools; Min Chen wrote the paper.

Conflicts of Interest

The authors declare no conflict of interest.

References

1. Jeon, W.G.; Chang, K.H.; Cho, Y.S. An equalization technique for orthogonal frequency-division multiplexing systems in time-variant multipath channel. *IEEE Trans. Commun.* **1999**, *47*, 27–32.
2. Cai, X.; Giannakis, G.B. Bounding performance and suppressing intercarrier interference in wireless mobile OFDM. *IEEE Trans. Commun.* **2003**, *51*, 2047–2056.
3. Liu, D.N.; Fitz, M.P. Iterative MAP equalization and decoding in wireless mobile coded OFDM. *IEEE Trans. Commun.* **2009**, *57*, 2042–2051.
4. Schniter, P. Low-complexity equalization of OFDM in doubly selective channels. *IEEE Trans. Signal Process.* **2004**, *52*, 1002–1011.
5. Rugini, L.; Banelli, P.; Leus, G. Low-complexity banded equalizer for OFDM systems in Doppler spread channels. *EURASIP J. Adv. Signal Process.* **2006**, *2006*, 1–13.
6. Tauböck, G.; Hampejs, M.; Švač, P.; Matz, G.; Hlawatsch, F.; Gröchenig, K. Low-complexity ICI/ISI equalization in doubly dispersive multicarrier systems using a decision-feedback LSQR algorithm. *IEEE Trans. Signal Process.* **2011**, *59*, 2432–2436.
7. Yerramalli, S.; Stojanovic, M.; Mitra, U. Partial FFT demodulation: A detection method for highly Doppler distorted OFDM systems. *IEEE Trans. Signal Process.* **2012**, *60*, 5906–5918.
8. Baracca, P.; Tomasin, S.; Vangelist, L.; Benvenuto, N.; Morello, A. Per sub-block equalization of very long OFDM blocks in mobile communications. *IEEE Trans. Commun.* **2011**, *59*, 363–368.
9. Tomasin, S.; Gorokhov, A.; Yang, H.; Linnartz, J.P. Iterative interference cancellation and channel estimation for mobile OFDM. *IEEE Trans. Wirel. Commun.* **2005**, *4*, 238–245.
10. Hwang, S.U.; Lee, J.H.; Seo, J. Low-complexity iterative ICI cancellation and equalization for OFDM systems over doubly selective channels. *IEEE Trans. Broadcast.* **2009**, *55*, 132–139.
11. De Lamare, R.C.; Sampaio-Neto, R. Minimum mean square error iterative successive parallel arbitrated decision feedback detectors for DS-CDMA systems. *IEEE Trans. Commun.* **2008**, *56*, 778–789.
12. Choi, J.W.; Singer, A.C.; Lee, J.; Cho, N.I. Improved linear soft-input soft-output detection via soft feedback successive interference cancellation. *IEEE Trans. Commun.* **2010**, *58*, 986–996.

13. Choi, J. Approximate MAP detection with ordering and successive processing for iterative detection and decoding in MIMO systems. *IEEE J. Sel. Top. Signal Process.* **2011**, *5*, 1415–1424.
14. Panayırçı, E.; Dogan, H.; Poor, H.V. Low-complexity MAP-based successive data detection for coded OFDM systems over highly mobile wireless channels. *IEEE Trans. Veh. Technol.* **2011**, *60*, 2849–2857.
15. Ochandiano, P.; Wymeersch, H.; Mendicute, M.; Martinez, L.; Sobron, I. Factor graph based detection approach for high-mobility OFDM systems with large FFT modes. *EURASIP J. Wirel. Commun. Netw.* **2012**, *2012*, 1–12.
16. Namboodiri, V.; Liu, H.; Spasojević, P. Low-complexity iterative receiver design for mobile OFDM systems. *EURASIP J. Adv. Signal Process.* **2012**, *2012*, doi:10.1186/1687-6180-2012-166.
17. Li, L.; Burr, A.G.; de Lamare, R.C. Joint iterative receiver design and multi-segmental channel estimation for OFDM systems over rapidly time-varying channels. In Proceedings of the IEEE Vehicular Technology Conference, Dresden, Germany, 2–5 June 2013.
18. Panayırçı, E.; Dogan, H.; Poor, H.V. Joint channel estimation, equalization, and data detection for OFDM systems in the presence of very high mobility. *IEEE Trans. Signal Process.* **2010**, *58*, 4225–4238.
19. Wang, H.W.; Lin, D.W.; Sang, T.H. OFDM signal detection in doubly selective channels with blockwise whitening of residual intercarrier interference and noise. *IEEE J. Sel. Areas Commun.* **2012**, *30*, 684–694.
20. Li, P.; de Lamare, R.C. Multiple feedback successive interference cancellation detection for multiuser MIMO systems. *IEEE Trans. Wirel. Commun.* **2011**, *10*, 2434–2439.
21. Geman, S.; Geman, D. Stochastic relaxation, Gibbs distribution and the Bayesian restoration of images. *IEEE Trans. Pattern Anal. Mach. Intell.* **1984**, *PAMI-6*, 721–741.
22. Huang, Y.; Djurić, P.M. Multiuser detection of synchronous code-division multiple access signals by perfect sampling. *IEEE Trans. Signal Process.* **2002**, *50*, 1724–1734.
23. Farhang-Boroujeny, B.; Zhu, H.; Shi, Z. Markov chain Monte Carlo algorithm for CDMA and MIMO Communication systems. *IEEE Trans. Signal Process.* **2006**, *54*, 1896–1909.
24. Aulin, T.M. Breadth-first maximum likelihood sequence detection: Basics. *IEEE Trans. Commun.* **1999**, *47*, 208–216.
25. Bahl, L.; Cocke, J.; Jelinek, F.; Raviv, J. Optimal decoding of linear codes for minimizing symbol error rate. *IEEE Trans. Inf. Theory* **1974**, *20*, 284–287.
26. Kay, S. *Fundamentals of Statistical Signal Processing: Estimation Theory*; Prentice-Hall: Upper Saddle River, NJ, USA, 1993.
27. Laraway, S.A.; Farhang-Boroujeny, B. Implementation of a Markov Chain Monte Carlo based Multiuser/MIMO detection. *IEEE Trans. Circuits Syst. I* **2009**, *56*, 246–255.
28. Li, Y.; Cimini, J. Bounds on the interchannel interference of OFDM in time-varying impairments. *IEEE Trans. Commun.* **2001**, *49*, 401–404.
29. Le, K.N.; Dabke, K. BER of OFDM with diversity and pulse shaping in Rayleigh fading environments. *Digit. Signal Process.* **2010**, *20*, 1687–1696.

30. Papoulis, A.; Pillai, S.U. *Probability, Random Variables, and Stochastic Processes*; Tata McGraw-Hill Education: Novida, India, 2002.
31. Tse, D.; Viswanath, P. *Fundamentals of Wireless Communication*; Cambridge University Press: Cambridge, UK, 2005.
32. Gradshteyn, I.S.; Ryzhik, I.M. *Tables of Integrals, Sums, Series, and Products*; Nauka: Moscow, Russia, 1971.
33. Yang, L.L. Receiver multiuser diversity aided multi-stage minimum mean-square error detection for heavily loaded DS-CDMA and SDMA systems. *IEEE Trans. Commun.* **2010**, *58*, 3397–3404.
34. Mostofi, Y.; Cox, D.C. ICI mitigation for pilot-aided OFDM mobile systems. *IEEE Trans. Wirel. Commun.* **2005**, *4*, 765–774.
35. Şenol, H.; Panayırçı, E.; Poor, H.V. Nondata-aided joint channel estimation and equalization for OFDM systems in very rapidly varying mobile channels. *IEEE Trans. Signal Process.* **2007**, *55*, 2226–2238.
36. Tang, Z.; Cannizzaro, R.C.; Leus, G. Pilot-assisted time-varying channel estimation for OFDM systems. *IEEE Trans. Signal Process.* **2007**, *55*, 2226–2238.
37. Choi, Y.S.; Voltz, P.J.; Cassara, F.A. On channel estimation and detection for multicarrier signals in fast and selective Rayleigh fading channels. *IEEE Trans. Commun.* **2001**, *49*, 1375–1387.

© 2015 by the authors; licensee MDPI, Basel, Switzerland. This article is an open access article distributed under the terms and conditions of the Creative Commons Attribution license (<http://creativecommons.org/licenses/by/4.0/>).